



# Unveiling the functional components and antivirulence activity of mustard leaves using an LC-MS/MS, molecular networking, and multivariate data analysis integrated approach

Rana M. Ibrahim<sup>a,\*</sup>, Basma M. Eltanany<sup>b</sup>, Laura Pont<sup>c,d</sup>, Fernando Benavente<sup>c,\*</sup>, Shahira A. ElBanna<sup>e</sup>, Asmaa M. Otify<sup>a</sup>

<sup>a</sup> Department of Pharmacognosy, Faculty of Pharmacy, Cairo University, Cairo 11562, Egypt

<sup>b</sup> Department of Analytical Chemistry, Faculty of Pharmacy, Cairo University, Cairo 11562, Egypt

<sup>c</sup> Department of Chemical Engineering and Analytical Chemistry, Institute for Research on Nutrition and Food Safety (INSA-UB), University of Barcelona, Barcelona 08028, Spain

<sup>d</sup> Serra Hünter Programe, Generalitat de Catalunya, Barcelona 08007, Spain

<sup>e</sup> Department of Microbiology and Immunology, Faculty of Pharmacy, Cairo University, Cairo 11562, Egypt

## ARTICLE INFO

### Keywords:

Brassica  
Mustard  
Chemometrics  
Metabolomics  
Molecular networking  
Antibacterial  
Antihemolytic  
*hla* transcription

## ABSTRACT

Plant extracts have recently received increased attention as alternative sources of antimicrobial agents in the fight against multidrug-resistant bacteria. Non-targeted metabolomics liquid chromatography-quadrupole time-of-flight tandem mass spectrometry, molecular networking, and chemometrics were used to evaluate the metabolic profiles of red and green leaves of two *Brassica juncea* (L.) varieties, var. *integrifolia* (IR and IG) and var. *rugosa* (RR and RG), as well as to establish a relationship between the elucidated chemical profiles and antivirulence activity. In total, 171 metabolites from different classes were annotated and principal component analysis revealed higher levels of phenolics and glucosinolates in var. *integrifolia* leaves and color discrimination, whereas fatty acids were enriched in var. *rugosa*, particularly trihydroxy octadecadienoic acid. All extracts demonstrated significant antibacterial activity against *Staphylococcus aureus* and *Enterococcus faecalis*, presenting the IR leaves the highest antihemolytic activity against *S. aureus* (99 % inhibition), followed by RR (84 %), IG (82 %), and RG (37 %) leaves. Antivirulence of IR leaves was further validated by reduction in alpha-hemolysin gene transcription (~4-fold). Using various multivariate data analyses, compounds positively correlated to bioactivity, primarily phenolic compounds, glucosinolates, and isothiocyanates, were also identified.

## 1. Introduction

*Brassica juncea* (L.), also known as Indian mustard or Brown mustard, is one of the most commonly cultivated *Brassica* crops for oil and condiment production, in addition to being valuable medicinal plants and edible vegetables that are widely consumed worldwide. Mustard breeding is underway to develop genotypes with low levels of glucosinolates and erucic acid for oil production (Merah, 2015). However, to

provide a hot flavor to the condiments, breeding varieties with high glucosinolates content, particularly sinigrin, is required. Because of such breeding programs, a large number of mustard varieties have been developed (Merah, 2015). Apart from the seeds, mustard leaves are highly valued because they account for a significant portion of the total weight of mustard plantations. Mustard greens are well known to contain several bioactive phytochemicals such as flavonoids, sterols, phenolic acids, and sulfur compounds. Traditionally, mustard leaves

**Abbreviations:** AUC, area under the ROC curve; CV-ANOVA, cross-validation residuals; GNPS-MN, global natural products social molecular networking; *hla*, alpha-hemolysin gene; IG, *Brassica juncea* (L.) var. *integrifolia* green leaves; IR, *Brassica juncea* (L.) var. *integrifolia* red leaves; LC-QTOF-MS/MS, liquid chromatography-quadrupole time-of-flight tandem mass spectrometry; MGDG, monogalactosyldiacylglycerol; MHA, Mueller-Hinton agar; MHB, Mueller-Hinton broth; PA, phosphatidic acid; PG, phosphatidyl glycerols; PI, phosphatidyl inositols; qPCR, quantitative polymerase chain reaction; RG, *Brassica juncea* (L.) var. *rugosa* green leaves; RMSEcv, root mean square error of cross-validation; RMSEE, root mean square error of estimation; ROC, receiver operating characteristic; RR, *Brassica juncea* (L.) var. *rugosa* red leaves; SQDG, sulfoquinovosyl diacylglycerol; SQMG, sulfoquinovosyl monoacylglycerol; TSB, tryptic soya broth; VIP, variable importance to projection.

\* Corresponding authors.

E-mail addresses: [rana.mohamed@pharma.cu.edu.eg](mailto:rana.mohamed@pharma.cu.edu.eg) (R.M. Ibrahim), [fbenavente@ub.edu](mailto:fbenavente@ub.edu) (F. Benavente).

<https://doi.org/10.1016/j.foodres.2023.112742>

Received 22 December 2022; Received in revised form 14 March 2023; Accepted 17 March 2023

Available online 21 March 2023

0963-9969/© 2023 The Authors. Published by Elsevier Ltd. This is an open access article under the CC BY-NC-ND license (<http://creativecommons.org/licenses/by-nc-nd/4.0/>).

have been used as diuretics, expectorants, and stimulants (Tian et al., 2021). Other potential health benefits of mustard leaves have been also reported, related to their anti-inflammatory, anti-obesity, antidiabetic, antioxidant, antidepressant, antibacterial, anticancer, and cardiovascular protective properties (Tian & Deng, 2020). Previous studies have attributed the ability of mustard plants to prevent some cancer types and cardiovascular diseases to the content of polyphenols, glucosinolates, and isothiocyanates (Tian & Deng, 2020). In addition, several authors have pointed to the importance of considering the differences at the level of the nutritional and bioactive components between the two most common color types of mustard leaves, red and green (Cuong et al., 2018). For instance, the red leaves of *B. juncea* (L.) var. *integrifolia* have showed better glucose-lowering effects than the green ones (Jo et al., 2018). Also red mustard leaves demonstrated higher anticancer activity than green mustard leaves (Kim et al., 2011).

Non-targeted metabolomics approaches based on liquid chromatography-mass spectrometry (LC-MS) have been widely used to find specific discriminatory markers for bioactive ingredients in plants (Zhang et al., 2021). Besides, such approaches can visualize the metabolic differences between several plant varieties, allowing their discrimination and classification (Younis et al., 2022). The most useful chemometric methods applied for chemical data processing and extraction of valuable information from large metabolomics datasets are principal component analysis (PCA) and orthogonal projection to latent structure-discriminant analysis (OPLS-DA), which derives from partial least squares-discriminant analysis (Younis et al., 2022). These chemometrics studies are completed with the identification of the detected compounds based on the MS information and database or literature search. Recently, molecular networking (MN) via the global natural products social molecular networking platform (GNPS), has demonstrated to be an excellent complement for the detailed analysis and exploration of MS metabolomics datasets. MN assists the annotation of different metabolite classes and analogs, and aid in isomers detection by mining spectral similarity between their tandem-mass spectrometry (MS/MS) fragmentation patterns (Hegazi, Khattab, Frolov, Wessjohann, & Farag, 2022).

Because the widespread use of antibiotics has increased bacterial multidrug resistance, there is a great need to look for novel antimicrobial agents through screening different resources, including plants. The structural diversity of plant-derived antimicrobial compounds is enormous (Andini et al., 2021). Among them, phenols, flavonoids, isothiocyanates, and glucosinolates have been recognized as potential antimicrobial candidates with a broad activity spectrum (Saavedra et al., 2010). They are naturally found in the Brassicaceae family and numerous studies have reported the antibacterial activity of many *Brassica* species (Jaiswal, Rajauria, Abu-Ghannam, & Gupta, 2012). Interestingly, few studies have highlighted the importance of mustard leaves as a source of antibacterial compounds (Verma, Tiwari, Jaiswal, & Pandey, 2022). Among the different bacterial species, *Staphylococcus aureus* presents a high probability of developing antibiotic resistance over time along with expressing various virulence factors (Grumann, Nubel, & Broker, 2014). Alpha-hemolysin, which is encoded by the alpha-hemolysin gene (*hla*), is considered as one of the staphylococcal virulence factors, being highly correlated with infection severity (Grumann et al., 2014). Alpha-hemolysin is a pore-forming protein that mainly causes the lysis of red blood cells, along with targeting some immune cells e.g., monocytes, macrophages, and neutrophils (Okba et al., 2022). Up to now, the antihemolytic activity of mustard leaves against *S. aureus* is still uncovered.

Here, a non-targeted metabolomics study is performed by liquid chromatography-quadrupole time-of-flight tandem mass spectrometry (LC-QTOF-MS/MS) followed by MN and multivariate data analysis to assess the metabolic differences between the red and green leaves of two *B. juncea* (L.) varieties, var. *integrifolia* (red, IR and green, IG) and var. *rugosa* (red, RR, and green, RG). Additionally, this study aims to determine the potential antibacterial and antivirulence activities of the four

mustard leaves against various Gram-positive and Gram-negative bacteria. The proposed strategy allows to better understand the complexities of mustard chemical profiles and to highlight metabolite variation among the mustard samples as a function of the variety and leaf color, as well as to identify the metabolite biomarkers correlated to the mustard bioactivities. Mustard leaves are revealed as a valuable source of specific antimicrobial compounds against the investigated Gram-positive bacteria, with marked *S. aureus* antihemolytic activity. These findings could be of interest in agri-food and pharmaceutical industries.

## 2. Materials and methods

### 2.1. Plant material and extraction

The red and green leaves of *B. juncea* (L.) var. *integrifolia* and var. *rugosa* were obtained from Makar Farm (Giza, Egypt) in March 2021. Herbarium vouchers (9.06.2022I & 9.06.2022II) were deposited at the herbarium of the Department of Pharmacognosy, Faculty of Pharmacy, Cairo University, Egypt. Air-dried mustard leaves (100 g each) were extracted separately using cold maceration (25 °C) in methanol (twice in 1 L each). Solvent extracts were evaporated until dryness in a rotary evaporator (50 °C) to obtain solid extracts that were then transferred to HPLC vials, and kept at -20°C till further analysis. Three biological replicates were prepared for each mustard sample and extracted in parallel under the same conditions.

### 2.2. LC-QTOF-MS/MS

LC-QTOF-MS/MS experiments were performed in a 1260 Infinity liquid chromatograph coupled to a 6546 LC/QTOF mass spectrometer with an orthogonal electrospray ionization (ESI) interface (Agilent Technologies, Waldbronn, Germany). Formic acid ( $\geq 95.0\%$ ), acetonitrile, water, and methanol (LC-MS grade) were supplied by Merck (Darmstadt, Germany).

For separation, a Zorbax SB-C18 column (150 mm total length ( $L_T$ )  $\times$  2.1 mm internal diameter (ID), 5  $\mu$ m particle size, 90 Å pore diameter, Agilent Technologies) was used. Experiments were performed with gradient elution at a flow rate of 350  $\mu$ L/min. Mobile phase solvents were (A) water and (B) acetonitrile (both with 0.1 % (v/v) of formic acid). Both were degassed for 10 min by sonication before use. The optimized elution gradient of solvent B was: 5 % (v/v) for 1 min and from 5 % to 95 % (v/v) in 15 min, followed by cleaning and re-equilibration steps at 95 % (v/v) for 2 min, from 95 % to 5 % (v/v) in 2 min, and finally 5 % (v/v) for 5 min. Samples were injected (5  $\mu$ L) using an autosampler refrigerated at 4 °C. Samples for LC/MS were prepared by dissolving 10 mg of the solid extracts in 1 mL of methanol, centrifuging at 13,000 g for 10 min, and filtering (syringe nylon filter 0.22  $\mu$ m pore diameter). Experiments were done in triplicate at room temperature. Instrument control, data acquisition, and processing for the LC part were performed with the ChemStation LC3D software (Agilent Technologies).

The Q-TOF mass spectrometer was operated under the optimized conditions in negative ESI mode using the following parameters: capillary voltage 3500 V, drying gas temperature and flow rate were 350 °C and 8 L/min, respectively, nebulizer gas 30 psi, fragmentor voltage 150 V, skimmer voltage 60 V, and OCT 1 RF Vpp voltage 300 V. The auto-MS/MS mode was applied over the  $m/z$  range of 50–2000 with an MS scan rate of 10 spectra/s and an MS/MS scan rate of 6 spectra/s. The collision energy was set according to the formula (slope)  $\times$  ( $m/z$ )/100 + offset, where the slope was 5, and the offset 10. The precursor selection was defined as follows: maximum precursor per cycle 9, absolute threshold 200 counts, relative threshold 0.01 %, purity stringency 100 %, purity cutoff 30 %, isotope model common organic molecules, active exclusion enabled but released after 2 spectra and after 0.5 min, precursors sorted by abundance only, and isolation window  $\sim$  1.3  $m/z$  (narrow). MassHunter software (Agilent Technologies) was used for

instrument control, data acquisition and processing of the MS/MS data. The raw data were converted to mzXML format using the open-source software MSConvert 3.0 (<https://www.proteowizard.org>). Then, the mzXML files were imported to the data mining open-source software MZmine 2.53 (<https://github.com/mzmine/mzmine2/releases/tag/v2.53>) for peak picking followed by deconvolution, deisotoping, alignment, and formula prediction (Ibrahim, Elmasry, Refaey, & El-Shiekh, 2022).

### 2.3. Molecular networking and metabolites annotation

The mzXML files were uploaded to the GNPS online platform to generate the online workflow. The created MN and its parameters can be accessed via the following link: (<https://gnps.ucsd.edu/ProteoSAFe/status.jsp?task=abee0988fe0f4366b20f76cebfa56cf5>). Network files were imported into the open-source software platform Cytoscape 3.9.1 (<https://cytoscape.org/download.html>) for additional processing and visualization.

### 2.4. Antibacterial activity and antihemolytic effect

#### 2.4.1. Bacterial strains

Six bacterial strains were used to evaluate the antibacterial activity, two strains were Gram-positive bacteria, *S. aureus* ATCC 6538 and *Enterococcus faecalis* ATCC 29212, while the remaining four strains were Gram-negative bacteria, including *Escherichia coli* K-12 MG1655, *Salmonella typhi* ATCC 35664, *Acinetobacter baumannii* ATCC 19606, and *Pseudomonas aeruginosa* PAO1.

#### 2.4.2. Determination of antibacterial activity

Antibacterial activity was determined by the agar well diffusion method (Gonelimali et al., 2018). First, the six strains were allowed to grow in Mueller-Hinton broth (MHB, Difco, USA) at 37 °C with shaking at 180 rpm. After 24 h of incubation, bacterial suspensions were diluted with MHB until reaching an optical density at 600 nm (OD600 0.08–0.1) equivalent to 0.5 MacFarland standard ( $\approx 1.5 \times 10^8$  CFU/mL). Mueller-Hinton agar (MHA) plates were then surface inoculated using cotton swabs loaded with the diluted cultures of the different strains. The MHA plates were perforated using a sterile cork pourer to form wells with diameters ranging from 10 to 11 mm.

The extracts stock solutions were prepared by dissolving 1.5 g of the solid extracts in 1 mL of dimethyl sulfoxide (DMSO, Sigma-Aldrich, Germany). Then, each well of the inoculated MHA was loaded with 150  $\mu$ L of the extract solution to reach a final concentration of 225 mg/well. For each bacterial strain, two different controls were done loading one well with 150  $\mu$ L DMSO and another one with 5  $\mu$ g of the reference synthetic antibiotic ciprofloxacin (Amriya Pharmaceutical Industries, Egypt) (Humphries et al., 2018). The diameter (mm) of the zone of inhibition of these extracts was measured and recorded.

#### 2.4.3. Determination of antihemolytic effect against *S. aureus*

The antihemolytic effect of the extracts was assessed using an hemolytic assay previously described with slight modifications (Okba et al., 2022). Overnight suspension of *S. aureus* was diluted 1:100 (v/v) in tryptic soya broth (TSB) so that the OD600 reached  $\sim 0.1$ . The culture was then divided into six test tubes and incubated for 18–20 h at 37°C with shaking at 180 rpm, with or without the tested extracts as follows: (i) first, *S. aureus* culture only, (ii) second, *S. aureus* culture supplied with DMSO, and (iii) third to sixth, *S. aureus* culture supplied with the four tested extracts, respectively. The sub-inhibitory concentrations of the extracts were used and added independently to the adjusted culture to a final concentration of 6.25 mg/mL. After 20 h incubation, the growth of *S. aureus* in the presence and absence of the tested extracts was recorded by measuring the OD600. Then, supernatants were collected after centrifugation to test for the hemolytic activity of *S. aureus* which was conducted using 4 % (v/v) rabbit blood (the used protocol was approved

by the Research Ethics Committee of Faculty of Pharmacy (REC-FOPCU), Cairo University (Approval code: MI3127). Briefly, 500  $\mu$ L of supernatants were mixed with equal volumes of 4 % (v/v) rabbit blood and incubated at 37°C in a water bath for 45 min. TSB supplemented with each of the corresponding tested extracts and mixed with an equal volume of 4 % (v/v) rabbit blood were used as blanks. In addition, sterile phosphate buffer saline and 1 % Triton X-100, were included as negative and positive hemolytic controls, respectively. Afterward, the blood-supernatant mixtures together with all controls were centrifuged at 22,000  $\times$  g for 5 min and the absorbance was measured at 540 nm (A540). The antihemolytic effect of the tested extracts was estimated by comparing the hemolytic activity of *S. aureus* in the presence and absence of extracts. To avoid variation caused by differences in growth, the actual hemolysis (AH) was calculated as the ratio of A540/OD600. In addition, the percentage of inhibition was calculated as follows:

$$\frac{\text{AH of } S. \text{ aureus without extracts } \left( \frac{A_{540}}{OD_{600}} \right) - \text{AH of } S. \text{ aureus with extract } \left( \frac{A_{540}}{OD_{600}} \right)}{\text{AH of } S. \text{ aureus without extracts } (A_{540}/OD_{600})} \times 100$$

#### 2.4.4. Transcriptional analysis of alpha-hemolysin gene (*hla*)

Optical density of overnight culture of *S. aureus* was estimated, and adjusted to 0.1 by dilution, then the culture was divided equally into three parts. IR and RG extracts were added to two cultures independently at a final concentration of 6.25 mg/mL, while DMSO was added to the third one as control. The three cultures were allowed to grow at 37°C and 180 rpm. Samples were collected at late exponential phase, and total RNA was extracted by RNeasy Mini kit (Qiagen, Germantown, MD, USA). cDNA was synthesized by the Promega Reverse Transcriptase Kit (Promega, Madison, WI, USA). *hla* transcriptional levels of the three cultures were estimated by quantitative polymerase chain reaction (qPCR). qPCR was performed in a Rotor-Gene-Q real-time PCR instrument (Qiagen), with a SensiFAST™ SYBR Lo-ROX Kit (Bioline Meridian Bioscience, TN, USA). *hla* primers were used for the quantification of the *hla* gene while 16S rRNA primers were used for amplification of the 16S rRNA housekeeping gene (Table S1). The relative quantitation of mRNA of *hla* gene was determined by the  $\Delta\Delta$ Ct method using Rotor-Gene-Q software (Livak & Schmittgen, 2001). The results were expressed as a fold change in *hla* message for cultures exposed to either IR or RG extracts relative to those exposed to the DMSO control.

#### 2.4.5. Statistical analysis

Statistical analyses of antibacterial and antihemolytic experiments were performed with GraphPad Prism 5 (GraphPad Software, San Diego, USA), and ANOVA followed by *post-hoc* multiple *t*-tests, with Holm-Sidak correction, was applied.

### 2.5. Multivariate data analysis

The aligned peak list for all the extract samples (3 replicates for each) obtained by MZmine software was exported as a CSV file, containing information about the feature ID number, retention time ( $t_r$ ), mass-to-charge ratio ( $m/z$ ), and peak intensity for each detected compound. A data matrix consisting of 12 columns (samples) and 1049 rows (peak intensity of each detected compound) was then mean-centered and imported into the SIMCA-P Version 14 (Umetrics, Umeå, Sweden). All variables were scaled to Pareto variance before PCA and OPLS-DA. Additionally, the web-based platform Metaboanalyst 5.0 (<https://www.metaboanalyst.ca/>) was used to find the most relevant metabolites correlated to the antihemolytic effect using Pearson's correlations in the pattern search function, variable importance to projection (VIP) from the OPLS-DA model, and the validated permutation test.

### 3. Results and discussion

#### 3.1. LC-QTOF-MS/MS metabolite profiling

The chemical profiles of the IG, IR, RG, and RR methanolic mustard leaf extracts were analyzed by LC-QTOF-MS/MS in the negative ESI mode to find possible metabolic differences between samples (*i.e.*, varieties and colors). The representative base peak chromatograms of the four extracts are shown in Fig. S1. After data processing for feature detection, a total of 1049 compounds were detected, of which 171 were tentatively identified. Identifications were based on accurate molecular mass and MS/MS fragment ions, and were further confirmed by searching in available literature and online databases with mzmine software *e.g.* KEGG (<https://www.genome.jp/kegg/compound/>), PubChem (<https://pubchem.ncbi.nlm.nih.gov/>), and lipidMaps (<https://www.lipidmaps.org/>) (Lin, Sun, Chen, & Harnly, 2011; Schmidt et al., 2010; Sun et al., 2013). Metabolites identification was further propagated with MN exploration, together with the proposed GNPS spectral library search. Information of the identified compounds:  $t_r$ ,  $m/z$  of the detected molecular ions, molecular formulas, fragment ions, compound classes, as well as putative identifications are summarized in Table 1. The putative structures of representative metabolites are shown in Fig. S2.

The identified metabolites (Table 1) belonged to various classes encompassing: 7 glucosinolates, 4 isothiocyanates, 45 flavonoids, 31 phenolic acids, and 23 fatty acids, besides, 1 coumarin, 1 aldehyde, 1 flavan-3-ol, and 4 organic acids. Additionally, 54 lipids from different classes were characterized for the first time in mustard leaf extracts including 10 phosphatidic acids (PA), 5 glycolipids, 7 phosphatidyl glycerols (PG), 8 phosphatidyl inositols (PI), and 24 sulfoglycolipids. The main identified secondary metabolites were phenolic compounds and flavonoids (a total of 76), agreeing with previous reports (Lin et al., 2011; Schmidt et al., 2010). The representative MS/MS spectra of a selected compound from each class are displayed as supplementary materials in Figs. S3-S14.

#### 3.2. Molecular networking-based categorization of mustard leaf metabolites

The established MN allowed the direct visual investigation of MS/MS data, alongside the observation of metabolite distribution among the different samples. Based on common MS/MS fragmentation patterns, it classified molecules into families or clusters. Molecules with similar fragmentation patterns are combined, while those with dissimilar fragmentation patterns are separated. Single nodes are used to represent molecules that do not form groups (Jouaneh et al., 2022). Accordingly, nodes were colored by sample type (*i.e.*, IR, IG, RR, and RG) and labeled with their precursor  $m/z$  values. Nodes were also displayed as a pie chart to reflect the semi-relative abundance of the detected molecular ions in the four extracts, while the edges indicated the mass differences between the connected nodes.

The MN (Fig. 1) contained 337 nodes comprising 18 clusters (minimum 2 connected nodes) and 107 self-looped nodes. Cluster A contained the identified flavonols and their acylated derivatives, while cluster B was mostly formed by the identified lipids. The identified fatty acids and glucosinolates were arranged in clusters C and D, respectively. Phenolic acids were grouped in clusters E, F, G, and H. Regarding self-looped nodes, mostly corresponded to organic acids, among other identified metabolites (Fig. 1).

##### 3.2.1. Identification of glucosinolates and isothiocyanates

Glucosinolates and isothiocyanates are sulfur-containing secondary metabolites commonly present in *B. juncea* (L.) (Tian & Deng, 2020). They are mainly responsible for the pungent flavor of the Brassicaceae plants. Isothiocyanates are considered the degradation byproducts of glucosinolates. Both are assumed to exhibit many biological effects, such

as anticancer, antioxidant, anti-inflammatory, and antimicrobial activities (Tian & Deng, 2020). Furthermore, glucosinolates can modulate insulin resistance and improve metabolic disorders in type 2 diabetes (Esteve, 2020). Intriguingly, MN (Fig. 1) unveiled the presence of a group of glucosinolates (cluster D) that were eluted early in the chromatographic separation and distributed mainly in IR and IG extracts (Fig. S1 and Table 1).

The main glucosinolate fragmentation occurs around the central isothiocyanate group and the formation of thioglucose fragment  $[C_6H_{11}O_5S]^-$  (Fig. S3). Besides, fragment ions are generated from the loss of the  $SO_3^-$  group and further loss of the glucose moiety. Other ions are formed by intramolecular rearrangements in which the sulfate group is transferred to the thioglucose moiety (Zhou et al., 2017). Following this fragmentation pathway (Fig. S3), seven glucosinolates were tentatively identified in the mustard leaf extracts (Table 1). For example, sinigrin (peak 1, Table 1 and Fig. S3) showed a molecular ion at  $m/z$  358.0269  $[C_{10}H_{16}NO_9S_2]$  and fragment ions at nominal  $m/z$  274, 259, 241, and 162. The other two fragments at  $m/z$  278 and 116, were assigned as the loss of  $SO_3^-$  and the further loss of glucose from this ion fragment, respectively (Fig. S3).

Four isothiocyanates (8, 13, 16, and 56, Table 1) were detected corresponding to allyl isothiocyanate, 8-(methylsulfinyl)octyl isothiocyanate, cleomin, and 9-(methylsulfinyl)nonyl isothiocyanate, respectively. The fragmentation of isothiocyanates involved the formation of isothiocyanate anion  $[N=C=S^-]$ ,  $m/z$  58 (Song, Iori, & Thornalley, 2006).

##### 3.2.2. Identification of phenolic acids and their derivatives

Numerous phenolic acids and their conjugates have been previously reported in mustard greens (Lin et al., 2011). They are mainly derivatives of hydroxycinnamic acids present as esters, glycosides, or glycoside-esters. In this study, 31 phenolic acids were identified, being coumaroyl-, caffeoyl-, sinapoyl-, feruloyl-, and hydroxyferuloyl- the main phenolic components. They were found mainly conjugated with quinic, shikimic, and malic acids, or as glycosides with one or more sugar units (Lin et al., 2011). The antioxidant, anti-inflammatory, antiproliferative, and preventative effects of mustard were reported to be related to the polyphenol content (Tian & Deng, 2020).

Phenolic acids were eluted after glucosinolates (Fig. S1) and constituted clusters E, F, G, and H in the MN, besides some scattered nodes (Fig. 1). Cinnamate esters showed higher abundance in IR and IG leaves than in RR and RG leaves as highlighted in the MN (Fig. 1). Cluster G (Fig. 1) revealed the presence of 2 cinnamate esters with quinic acid. They were annotated as 4-caffeoyl quinic acid (36, Fig. S4) and 3-*p*-coumaroyl quinic acid (60, Fig. S5) with  $[M-H]^-$  at  $m/z$  353.0870 and 337.0922, respectively. Compound 36 revealed product ions at nominal  $m/z$  191, 179, 147, and 135 corresponding to quinic acid, caffeic acid, and their decarboxylated ions, respectively. While, peak 60 showed fragment ions at nominal  $m/z$  191, 163, and 119 due to the production of quinic ion, coumaric ion, and further loss of the  $CO_2$  group, respectively (Table 1). The intensities of the fragment ions were in agreement with the reported data and confirmed the assignment of the esterification position (R. Jaiswal, Sovdat, Vivan, & Kuhnert, 2010).

Cluster H (Fig. 1) is composed of 2 nodes, the first one was assigned for feruloyl hexoside (61, Table 1) and the second showed a molecular ion with a  $m/z$  difference of 114. Inspection of the MS/MS spectrum of this compound (Fig. S6) led to its putative annotation as feruloyl oxylinolenic acid (139, Table 1)  $[m/z$  469.2586,  $C_{28}H_{37}O_6]$ . It exhibited fragment ions due to fatty acid (hydroxy linolenic acid, nominal  $m/z$  293) and ferulic acid (nominal  $m/z$  193). The occurrence of ferulic acid conjugated to hydroxylated fatty acids is widely common in plant cell walls as a component of the cuticle and suberin, so playing a vital role in providing rigidity to the cell wall and synthesis of other secondary metabolites (Kumar & Pruthi, 2014). Malate esters of hydroxyferulic, caffeic, coumaric, sinapic, and ferulic acids were detected mostly in cluster F (34, 64, 73, 76, and 79, respectively, Table 1, Fig. 1). In their

**Table 1**  
Compounds identified in the methanolic extracts of *B. juncea* (L.) samples by LC-QTOF-MS/MS in negative ESI mode.

Peak num.	$t_r$ (min)	Molecular ion (M-H) (m/z)	Molecular ion formula	Error ppm	MS/MS fragments (m/z)	Identification	Compound class	Source			
								IR	IG	RR	RG
1	1.03	358.0269	C <sub>10</sub> H <sub>16</sub> NO <sub>9</sub> S <sub>2</sub> <sup>-</sup>	-0.8	274, 259, 241, 162, 116, 96, 95, 74	Sinigrin	Gucosinolate	+	+	-	-
2	1.08	133.0142	C <sub>4</sub> H <sub>5</sub> O <sub>5</sub> <sup>-</sup>	-0.2	115, 71	Malic acid	Organic acid	+	+	+	+
3	1.29	153.0192	C <sub>7</sub> H <sub>5</sub> O <sub>4</sub> <sup>-</sup>	-0.7	109	Protocatechuic acid	Phenolic acid	-	-	+	-
4	1.41	191.0566	C <sub>7</sub> H <sub>11</sub> O <sub>6</sub> <sup>-</sup>	-2.5	173, 127, 85	Quinic acid	Organic acid	+	+	-	-
5	1.44	191.0196	C <sub>6</sub> H <sub>7</sub> O <sub>7</sub> <sup>-</sup>	-0.5	111, 87, 76, 57	Citric acid	Organic acid	+	+	-	-
6	1.50	163.0398	C <sub>9</sub> H <sub>7</sub> O <sub>3</sub> <sup>-</sup>	-1.5	119	p-Coumaric acid	Phenolic acid	+	+	+	+
7	1.56	372.0421	C <sub>11</sub> H <sub>18</sub> NO <sub>9</sub> S <sub>2</sub> <sup>-</sup>	-2.2	322, 274, 292, 259, 241, 176, 127	Gluconapin	Gucosinolate	+	+	-	-
8	1.77	98.007	C <sub>4</sub> H <sub>4</sub> NS <sup>-</sup>	0.3	96, 95, 78, 58	Allyl isothiocyanate	Isothiocyanate	-	+	-	-
9	1.94	374.0565	C <sub>11</sub> H <sub>20</sub> NO <sub>9</sub> S <sub>2</sub> <sup>-</sup>	-5.3	320, 302, 259, 161, 112, 96, 68	Glucocochlearin	Gucosinolate	+	+	-	-
10	2.06	414.0872	C <sub>14</sub> H <sub>24</sub> NO <sub>9</sub> S <sub>2</sub> <sup>-</sup>	-6.2	259, 206, 172, 144, 96	6-Heptenyl glucosinolate	Gucosinolate	+	-	-	-
11	2.15	374.0577	C <sub>11</sub> H <sub>20</sub> NO <sub>9</sub> S <sub>2</sub> <sup>-</sup>	-2.1	312, 274, 259, 241, 214, 180, 150	Butyl glucosinolate	Gucosinolate	-	+	-	-
12	2.32	374.0584	C <sub>11</sub> H <sub>20</sub> NO <sub>9</sub> S <sub>2</sub> <sup>-</sup>	-0.2	341, 312, 274, 259, 241, 214, 180, 150	Glucoconringianin	Gucosinolate	+	+	-	-
13	2.62	232.0822	C <sub>10</sub> H <sub>8</sub> NOS <sub>2</sub> <sup>-</sup>	-5.6	160, 103, 94, 78, 58	8-(Methylsulfinyl)octyl isothiocyanate	Isothiocyanate	-	+	-	-
14	3.22	147.0449	C <sub>9</sub> H <sub>7</sub> O <sub>2</sub> <sup>-</sup>	-1.6	113	Cinnamic acid	Phenolic acid	+	-	+	+
15	3.99	477.0628	C <sub>17</sub> H <sub>21</sub> N <sub>2</sub> O <sub>10</sub> S <sub>2</sub> <sup>-</sup>	-3.1	351, 330, 315, 274, 259, 241, 202, 173	4-Methoxy glucobrassicin	Gucosinolate	+	+	-	-
16	4.02	144.0663	C <sub>6</sub> H <sub>10</sub> NOS <sup>-</sup>	-2	96, 95, 86, 58	Cleomin	Isothiocyanate	+	+	+	-
17	5.25	305.0677	C <sub>15</sub> H <sub>13</sub> O <sub>7</sub> <sup>-</sup>	3.4	304, 282, 203, 168	(epi)Gallocatechin	Flavan-3-ol	+	+	+	+
18	6.27	949.2450	C <sub>39</sub> H <sub>49</sub> O <sub>27</sub> <sup>-</sup>	-1.7	787, 462, 299	Quercetin-3-O-trihexoside-7-O-hexoside	Flavonoid	+	-	+	-
19	6.45	299.0763	C <sub>13</sub> H <sub>15</sub> O <sub>8</sub> <sup>-</sup>	-3.1	137, 109, 93	Salicylic acid-O-hexoside	Phenolic acid	+	+	-	-
20	6.48	933.2289	C <sub>42</sub> H <sub>45</sub> O <sub>24</sub> <sup>-</sup>	-1.8	771, 609, 446, 249, 284, 179	Kaempferol-3-O-caffeoyl dihexoside-7-O-hexoside	Flavonoid	+	-	+	-
21	6.56	787.1926	C <sub>33</sub> H <sub>39</sub> O <sub>22</sub> <sup>-</sup>	-1.6	716, 581, 462, 299, 183	Quercetin-3-O-dihexoside-7-O-hexoside	Flavonoid	+	+	+	+
22	6.6	1111.2953	C <sub>45</sub> H <sub>59</sub> O <sub>30</sub> <sup>-</sup>	-3.7	949, 787, 609, 462, 299	Quercetin-3-O-trihexoside-7-O-dihexoside	Flavonoid	+	-	-	-
23	6.72	371.0991	C <sub>16</sub> H <sub>19</sub> O <sub>10</sub> <sup>-</sup>	2	209, 177, 159	Hydroxyferulic acid-O-hexoside	Phenolic acid	+	+	-	-
24	6.73	1287.3430	C <sub>55</sub> H <sub>67</sub> O <sub>35</sub> <sup>-</sup>	-2.7	933, 836, 591, 285, 191	Kaempferol-3-O-hydroxy feruloyl trihexoside-7-O-dihexoside	Flavonoid	+	+	-	-
25	6.77	771.1917	C <sub>33</sub> H <sub>39</sub> O <sub>21</sub> <sup>-</sup>	-2.3	723, 616, 516, 446, 371, 284, 261, 208, 151	Kaempferol-3-O-dihexoside-7-O-hexoside	Flavonoid	-	-	+	+
26	6.77	1125.2910	C <sub>49</sub> H <sub>57</sub> O <sub>30</sub> <sup>-</sup>	-2.4	949, 787, 462, 299, 176	Quercetin-3-O-feruloyl dihexoside-7-O-dihexoside	Flavonoid	+	+	-	-
27	6.80	979.2346	C <sub>43</sub> H <sub>47</sub> O <sub>26</sub> <sup>-</sup>	-1.5	787, 625, 462, 299	Quercetin-3-O-hydroxy feruloyl trihexoside	Flavonoid	+	+	-	-
28	6.82	1257.3330	C <sub>54</sub> H <sub>65</sub> O <sub>34</sub> <sup>-</sup>	-2.3	1095, 933, 753, 628, 285, 179, 161	Kaempferol-3-O-caffeoyl trihexoside-7-O-dihexoside	Flavonoid	+	+	-	-
29	6.86	1095.2807	C <sub>48</sub> H <sub>55</sub> O <sub>29</sub> <sup>-</sup>	-2.5	933, 771, 591, 446, 284, 178, 161	Kaempferol-3-O-caffeoyl trihexoside-7-O-hexoside	Flavonoid	+	+	-	-
30	6.86	1095.2807	C <sub>48</sub> H <sub>55</sub> O <sub>29</sub> <sup>-</sup>	-2.5	949, 933, 771, 721, 577, 299, 161	Quercetin-3-O-coumaroyl trihexoside-7-O-hexoside	Flavonoid	+	+	-	-
31	6.92	949.2232	C <sub>42</sub> H <sub>45</sub> O <sub>25</sub> <sup>-</sup>	-2.4	865, 607, 462, 300, 163	Quercetin-3-O-caffeoyl hexoside-7-O-dihexoside	Flavonoid	+	+	-	-
32	7.01	503.1399	C <sub>21</sub> H <sub>27</sub> O <sub>14</sub> <sup>-</sup>	-1.0	179, 161, 143	Caffeic acid-O-dihexoside	Phenolic acid	-	+	-	-
33	7.01	1155.3020	C <sub>50</sub> H <sub>59</sub> O <sub>31</sub> <sup>-</sup>	-2.6	906, 787, 621, 435, 299	Quercetin-3-O-sinapoyl trihexoside-7-O-hexoside	Flavonoid	-	+	+	-
34	7.04	325.0559	C <sub>14</sub> H <sub>13</sub> O <sub>9</sub> <sup>-</sup>	-1.8	209, 194, 150, 133, 115	Hydroxyferuloyl malate	Phenolic acid	-	+	-	-
35	7.07	577.1472	C <sub>27</sub> H <sub>29</sub> O <sub>14</sub> <sup>-</sup>	-5.6	300	Kaempferide-7-O-rhamnosyl pentoside	Flavonoid	+	-	-	-
36	7.09	353.0870	C <sub>16</sub> H <sub>17</sub> O <sub>9</sub> <sup>-</sup>	-2.2	291, 191, 179, 147, 135	4-Caffeoyl quinic acid	Phenolic acid	+	+	-	-
37	7.14	625.1398	C <sub>27</sub> H <sub>29</sub> O <sub>17</sub> <sup>-</sup>	-1.9	462, 299	Quercetin-3-O-dihexoside	Flavonoid	+	+	+	+
38	7.15	1271.347	C <sub>55</sub> H <sub>67</sub> O <sub>34</sub> <sup>-</sup>	-3.6	1109, 933, 915, 284	Kaempferol-3-O-feruloyl trihexoside-7-O-dihexoside	Flavonoid	-	+	-	-
39	7.19	1141.286	C <sub>49</sub> H <sub>57</sub> O <sub>31</sub> <sup>-</sup>	-2.5	979, 949, 787, 635, 462, 299, 178	Quercetin-3-O-hydroxy feruloyl trihexoside-7-O-hexoside	Flavonoid	+	+	-	-
40	7.20	801.2087	C <sub>34</sub> H <sub>41</sub> O <sub>22</sub> <sup>-</sup>	-1	639, 476, 434, 394, 315, 300, 151	Isorhamnetin-3-O-dihexoside-7-O-hexoside	Flavonoid	+	+	+	+
41	7.20	993.2500	C <sub>44</sub> H <sub>49</sub> O <sub>26</sub> <sup>-</sup>	-1.7	655, 625, 462, 299, 209, 178, 127	Quercetin-3-O-sinapoyl dihexoside-7-O-hexoside	Flavonoid	+	+	-	-
42	7.21	801.1870	C <sub>37</sub> H <sub>37</sub> O <sub>20</sub> <sup>-</sup>	-2	739, 639, 284, 191, 176	Kaempferol-3-O-hydroxy feruloyl dihexoside	Flavonoid	-	+	-	-
43	7.24	963.2396	C <sub>43</sub> H <sub>47</sub> O <sub>25</sub> <sup>-</sup>	-1.6	787, 625, 462, 299, 191, 175, 162	Quercetin-3-O-feruloyl dihexoside-7-O-hexoside	Flavonoid	-	-	+	-
44	7.27	319.0815	C <sub>16</sub> H <sub>15</sub> O <sub>7</sub> <sup>-</sup>	-2.5	241, 199, 161, 155, 109	Coumaroyl shikimate	Phenolic acid	-	-	-	+

(continued on next page)

Table 1 (continued)

Peak num.	$t_r$ (min)	Molecular ion (M-H) (m/z)	Molecular ion formula	Error ppm	MS/MS fragments (m/z)	Identification	Compound class	Source			
								IR	IG	RR	RG
45	7.27	1109.2959	C <sub>49</sub> H <sub>57</sub> O <sub>29</sub>	-2.9	771, 284, 255, 193, 178, 151	Kaempferol-3-O-feruloyl-trihexoside-7-O-hexoside	Flavonoid	+	+	-	-
46	7.31	1079.2854	C <sub>48</sub> H <sub>55</sub> O <sub>28</sub>	-2.9	917, 771, 753, 609, 284, 163	Kaempferol-3-O-coumaroyl dihexoside-7-O-dihexoside	Flavonoid	+	+	-	-
47	7.34	933.2497	C <sub>39</sub> H <sub>49</sub> O <sub>26</sub>	-2.2	771, 609, 446, 284, 251, 215, 161	Kaempferol-3-O-trihexoside-7-O-hexoside	Flavonoid	-	+	-	+
48	7.36	547.1637	C <sub>23</sub> H <sub>31</sub> O <sub>15</sub>	0.9	383, 223, 206, 190, 164	Sinapic acid-O-dihexoside	Phenolic acid	+	+	+	+
49	7.42	193.0507	C <sub>10</sub> H <sub>9</sub> O <sub>4</sub>	0.5	175, 160, 134	Ferulic acid	Phenolic acid	+	+	+	+
50	7.44	639.1557	C <sub>28</sub> H <sub>31</sub> O <sub>17</sub>	-1.8	315, 314, 300	Isorhamnetin-7-O-dihexoside	Flavonoid	+	+	+	+
51	7.48	947.2437	C <sub>43</sub> H <sub>47</sub> O <sub>24</sub>	-2.7	785, 609, 446, 284, 176, 151	Kaempferol-3-O-feruloyl dihexoside-7-O-hexoside	Flavonoid	+	+	-	+
52	7.53	1139.3093	C <sub>50</sub> H <sub>59</sub> O <sub>30</sub>	-1	977, 771, 429, 284, 205	Kaempferol-3-O-sinapoyl trihexoside-7-O-hexoside	Flavonoid	+	+	-	-
53	7.54	977.2565	C <sub>44</sub> H <sub>49</sub> O <sub>25</sub>	-0.3	815, 609, 489, 284, 129	Kaempferol-3-O-sinapoyl dihexoside-7-O-hexoside	Flavonoid	+	+	-	-
54	7.56	917.2332	C <sub>42</sub> H <sub>45</sub> O <sub>23</sub>	-2.7	755, 609, 447, 284	Kaempferol-3-O-coumaroyl dihexoside-7-O-hexoside	Flavonoid	-	+	-	-
55	7.56	323.0765	C <sub>15</sub> H <sub>15</sub> O <sub>8</sub>	-2.2	160	Umbelliferone-O-hexoside	Coumarin	+	-	-	-
56	7.56	246.0964	C <sub>11</sub> H <sub>29</sub> NOS <sub>2</sub>	-7.2	166, 110, 96, 58	9-(Methylsulfinyl)nonyl isothiocyanate	Isothiocyanate	+	+	-	-
57	7.57	209.0452	C <sub>10</sub> H <sub>9</sub> O <sub>5</sub>	-1.5	193, 157, 119	Hydroxyferulic acid	Phenolic acid	-	+	-	-
58	7.68	771.1997	C <sub>33</sub> H <sub>39</sub> O <sub>21</sub>	1	463, 446, 301	Quercetin-3-O-dihexoside-7-O-rhamnoside	Flavonoid	+	+	-	+
59	7.72	173.0452	C <sub>7</sub> H <sub>9</sub> O <sub>5</sub>	-1.9	156, 121, 104	Shikimic acid	Organic acid	-	+	-	-
60	7.72	337.0922	C <sub>16</sub> H <sub>17</sub> O <sub>8</sub>	-2	191, 163, 119	3-p-Coumaroyl quinic acid	Phenolic acid	+	+	+	+
61	7.76	355.1037	C <sub>16</sub> H <sub>19</sub> O <sub>9</sub>	0.8	258, 193, 178, 134	Feruloyl hexoside	Phenolic acid	+	+	+	-
62	7.87	741.1884	C <sub>32</sub> H <sub>37</sub> O <sub>20</sub>	0.1	608, 433, 300, 299	Quercetin-3-O-pentoside-7-O-rhamnosyl hexoside	Flavonoid	+	-	-	-
63	7.87	269.0479	C <sub>15</sub> H <sub>9</sub> O <sub>5</sub>	8.8	253, 243, 213, 195, 185, 130	Apigenin	Flavonoid	+	-	-	+
64	7.97	295.0455	C <sub>13</sub> H <sub>11</sub> O <sub>8</sub>	-1.4	194, 179, 135, 133, 115	Caffeoyl malate	Phenolic acid	+	+	-	-
65	8.21	385.1131	C <sub>17</sub> H <sub>21</sub> O <sub>10</sub>	-1.8	267, 249, 175, 135, 113	MGDG(8:4)	Glycolipid	+	+	-	-
66	8.21	385.1133	C <sub>17</sub> H <sub>21</sub> O <sub>10</sub>	-1.8	223, 205, 190, 164, 149	Sinapoyl hexoside	Phenolic acid	+	+	+	+
67	8.23	593.1509	C <sub>27</sub> H <sub>29</sub> O <sub>15</sub>	-0.5	446, 431, 285, 244, 124	Kaempferol-3-O-rhamnosyl-7-O-hexoside	Flavonoid	+	+	+	+
68	8.24	609.1438	C <sub>27</sub> H <sub>29</sub> O <sub>16</sub>	-3.7	447, 285, 283	Kaempferol-3,7-di-O-hexoside	Flavonoid	+	+	+	+
69	8.55	815.2031	C <sub>38</sub> H <sub>39</sub> O <sub>20</sub>	-1.1	680, 591, 284, 255, 190, 180, 150, 114	Kaempferol-3-O-sinapoyl dihexoside	Flavonoid	-	+	-	+
70	8.56	463.0874	C <sub>21</sub> H <sub>19</sub> O <sub>12</sub>	-1.7	301, 151	Quercetin-7-O-hexoside	Flavonoid	+	+	-	-
71	8.59	463.0866	C <sub>21</sub> H <sub>19</sub> O <sub>12</sub>	-3.4	300, 271, 239	Quercetin-3-O-hexoside	Flavonoid	+	+	+	-
72	8.71	739.2081	C <sub>33</sub> H <sub>39</sub> O <sub>19</sub>	-1.3	659, 523, 415, 223, 209, 205, 191, 178, 164, 149, 135	Sinapoyl hydroxy feruloyl dihexoside	Phenolic acid	+	+	-	-
73	8.73	279.0507	C <sub>13</sub> H <sub>11</sub> O <sub>7</sub>	-1.1	163, 119, 71	Coumaroyl malate	Phenolic acid	+	+	+	-
74	8.73	831.2017	C <sub>38</sub> H <sub>39</sub> O <sub>21</sub>	3.4	710, 601, 452, 315, 165	Isorhamnetin-3-O-feruloyl dihexoside	Flavonoid	+	-	-	-
75	8.82	755.1831	C <sub>36</sub> H <sub>35</sub> O <sub>18</sub>	0.3	699, 480, 285, 109	Kaempferol-3-O-coumaroyl dihexoside	Flavonoid	-	-	-	+
76	8.88	339.0722	C <sub>15</sub> H <sub>15</sub> O <sub>9</sub>	0.2	223, 205, 179, 164, 149	Sinapoyl malate	Phenolic acid	+	+	+	-
77	8.91	341.0879	C <sub>15</sub> H <sub>17</sub> O <sub>9</sub>	0.3	306, 241, 179, 161, 135	Caffeic acid-O-hexoside	Phenolic acid	+	+	+	-
78	8.99	223.0611	C <sub>11</sub> H <sub>11</sub> O <sub>5</sub>	-0.3	205, 190, 149	Sinapic acid	Phenolic acid	+	+	+	+
79	9.05	309.0613	C <sub>14</sub> H <sub>13</sub> O <sub>8</sub>	-0.9	193, 134	Feruloyl malate	Phenolic acid	+	+	+	+
80	9.07	477.1027	C <sub>22</sub> H <sub>21</sub> O <sub>12</sub>	-2.4	314, 299, 285, 257, 271, 257, 243, 151	Isorhamnetin-3-O-hexoside	Flavonoid	+	+	+	+
81	9.04	447.0922	C <sub>21</sub> H <sub>19</sub> O <sub>11</sub>	-2.4	285, 151	Kaempferol-7-O-hexoside	Flavonoid	+	+	+	+
82	9.08	447.0927	C <sub>21</sub> H <sub>19</sub> O <sub>11</sub>	-1.3	284, 255, 227, 151	Kaempferol-3-O-hexoside	Flavonoid	-	+	-	-
83	9.07	845.2118	C <sub>39</sub> H <sub>41</sub> O <sub>21</sub>	-3.3	665, 477, 314, 223, 209, 198, 101	Isorhamnetin-3-O-sinapoyl dihexoside	Flavonoid	+	-	-	-
84	9.21	753.2236	C <sub>34</sub> H <sub>41</sub> O <sub>19</sub>	-1.5	529, 223, 205, 190	Disinapoyl dihexoside	Phenolic acid	+	+	-	-
85	9.22	945.266	C <sub>44</sub> H <sub>49</sub> O <sub>23</sub>	-1	621, 427, 209, 205, 191, 157, 119	Disinapoyl hydroxy feruloyl dihexoside	Phenolic acid	+	+	-	-
86	9.23	723.2129	C <sub>33</sub> H <sub>39</sub> O <sub>18</sub>	1.7	399, 223, 193, 164, 134	Sinapoyl feruloyl dihexoside	Phenolic acid	+	+	-	-
87	9.32	693.2012	C <sub>32</sub> H <sub>37</sub> O <sub>17</sub>	-3.5	369, 193, 175, 134	Diferuloyl dihexoside	Phenolic acid	+	-	-	-
88	9.36	723.4296	C <sub>36</sub> H <sub>67</sub> O <sub>12</sub> S <sup>-</sup>	-8.6	225, 165, 153, 95, 81	SQDG(27:0)	Sulfoglycolipid	+	+	+	+
89	9.49	187.0974	C <sub>9</sub> H <sub>15</sub> O <sub>4</sub>	-0.8	169, 125, 97	Nonanedioic acid	Fatty acid	+	-	+	+
90	9.56	447.0927	C <sub>21</sub> H <sub>19</sub> O <sub>11</sub>	-1.3	301	Quercetin-7-O-rhamnoside	Flavonoid	+	+	-	+
91	9.64	959.2803	C <sub>38</sub> H <sub>55</sub> O <sub>28</sub>	-8.6	223, 205, 190	Trisinapoyl dihexoside	Phenolic acid	+	+	-	-
92	9.71	591.1699	C <sub>28</sub> H <sub>31</sub> O <sub>14</sub>	-3.4	385, 223, 208, 191, 149	Disinapoyl hexoside	Phenolic acid	+	+	-	-
93	9.71	299.1860	C <sub>16</sub> H <sub>27</sub> O <sub>5</sub>	-1.2	280, 255, 237	Oxo-hexadecanedioic acid	Fatty acid	-	+	+	+
94	9.77	929.2683	C <sub>44</sub> H <sub>49</sub> O <sub>22</sub>	-4.1	735, 223, 205, 193, 190, 175, 160, 125	Disinapoyl Feruloyl dihexoside	Phenolic acid	+	+	-	-
95	10.4	201.1133	C <sub>10</sub> H <sub>17</sub> O <sub>4</sub>	0.4	139	Dihydroxy decanoic acid	Fatty acid	+	+	+	+
96	10.9	327.2172	C <sub>18</sub> H <sub>31</sub> O <sub>5</sub>	-1.4	217, 162, 132	Trihydroxy octadecadienoic acid	Fatty acid	+	+	+	+

(continued on next page)

Table 1 (continued)

Peak num.	$t_r$ (min)	Molecular ion (M-H) (m/z)	Molecular ion formula	Error ppm	MS/MS fragments (m/z)	Identification	Compound class	Source			
								IR	IG	RR	RG
97	10.9	677.4232	$C_{38}H_{63}O_8P^-$	6.6	416, 327, 291, 273, 261, 251, 233, 209	PA(35:6)	Phosphatidic acid	+	+	+	+
98	10.97	211.1338	$C_{12}H_{19}O_3^-$	-0.7	184	Hydroxy dodecadienoic acid	Fatty acid	+	+	+	+
99	11.4	329.2331	$C_{18}H_{33}O_5^-$	-0.7	293, 201, 171	Trihydroxy octadecenoic acid	Fatty acid	+	+	+	+
100	11.46	445.1133	$C_{22}H_{21}O_{10}^-$	-1.6	401, 387, 357, 341 326, 203, 189	Disinapic acid	Phenolic acid	+	+	-	-
101	11.54	315.0507	$C_{16}H_{11}O_7^-$	-1	300, 151	Isorhamnetin	Flavonoid	+	+	+	+
102	11.73	549.2360	$C_{25}H_{41}O_{11}S^-$	-2.5	225, 165, 153, 95, 81	SQMG(16:3)	Sulfoglycolipid	+	+	-	+
103	12.42	593.2700	$C_{27}H_{45}O_{12}S^-$	4.7	225, 165, 153, 95, 81	SQDG(18:2)	Sulfoglycolipid	+	+	-	+
104	12.42	593.2689	$C_{27}H_{46}O_{12}P^-$	6.6	277, 259, 241, 171, 151	PI(18:3)	Phosphatidyl inositol	+	+	+	+
105	12.53	577.2681	$C_{27}H_{45}O_{11}S^-$	-1.2	225, 81	SQMG(18:3)	Sulfoglycolipid	+	+	+	+
106	12.54	185.1188	$C_{10}H_{17}O_3^-$	2.7	173, 164, 149, 129	Hydroxy decenoic acid	Fatty acid	-	-	+	+
107	12.54	307.1908	$C_{18}H_{27}O_4^-$	-2.1	263, 235, 211, 119	Hydroxy oxo-octadecatrienoic acid	Fatty acid	+	+	+	+
108	12.70	553.2679	$C_{25}H_{45}O_{11}S^-$	-1.6	225, 165, 153, 95, 81	SQMG(16:1)	Sulfoglycolipid	+	+	-	-
109	12.96	595.2835	$C_{27}H_{48}O_{12}P^-$	-9	279, 241, 223, 152, 78	PI(18:2)	Phosphatidyl inositol	+	+	+	+
110	13.02	579.2835	$C_{27}H_{47}O_{11}S^-$	-1.6	225, 81	SQMG(18:2)	Sulfoglycolipid	+	+	+	+
111	13.04	581.2986	$C_{27}H_{49}O_{11}S^-$	-2.2	225, 165, 153, 95, 81	SQMG(18:1)	Sulfoglycolipid	-	-	-	+
112	13.35	571.2880	$C_{25}H_{48}O_{12}P^-$	-1.5	475, 391, 255, 152	PI(16:0)	Phosphatidyl inositol	+	+	-	-
113	13.36	675.3575	$C_{33}H_{55}O_{14}^-$	-3.3	397, 318, 277, 233, 220, 159, 143	MGDG(18:3)	Glycolipid	+	-	-	+
114	13.39	555.2837	$C_{25}H_{47}O_{11}S^-$	-1.1	225, 81	SQMG(16:0)	Sulfoglycolipid	+	+	-	+
115	13.56	583.3142	$C_2H_{50}O_{11}S^-$	-2.5	225, 165, 153, 95, 81	SQMG(18:0)	Sulfoglycolipid	+	-	-	+
116	13.70	247.1697	$C_{16}H_{23}O_2^-$	-2.9	194, 151, 102	Hexadecatetraenoic acid	Fatty acid	+	+	+	+
117	13.71	505.3008	$C_{25}H_{45}O_{10}^-$	-2.2	255, 225, 189, 130	MGDG(16:0)	Glycolipid	+	+	-	+
118	13.73	505.2562	$C_{24}H_{42}O_9P^-$	-1.9	277, 152, 96, 78	PG(18:3)	Phosphatidyl glycerol	+	+	+	+
119	13.95	569.2987	$C_{26}H_{49}O_{11}S^-$	-2.4	225, 165, 153, 95, 81	SQMG(17:0)	Sulfoglycolipid	+	+	+	-
120	14.59	315.2533	$C_{18}H_{35}O_4^-$	-2.4	297, 276, 200, 171, 119	Dihydroxy stearic acid	Fatty acid	+	-	-	-
121	14.60	507.2718	$C_{24}H_{44}O_9P^-$	-2	279, 227, 152	PG(18:2)	Phosphatidyl glycerol	+	+	+	+
122	14.74	599.3188	$C_{27}H_{52}O_{12}P^-$	-2.3	315, 283, 259, 241, 152, 96, 78	PI(18:0)	Phosphatidyl inositol	+	+	-	-
123	14.80	527.2848	$C_{27}H_{43}O_{10}^-$	-2.6	277, 249, 187	MGDG(18:3)	Glycolipid	+	+	-	+
124	14.81	309.2065	$C_{18}H_{29}O_4^-$	-2	270, 241, 181, 167	Hydroxy oxo-octadecadienoic acid	Fatty acid	+	+	-	-
125	14.92	293.2119	$C_{18}H_{29}O_3^-$	-1	275, 183, 97	Hydroxy linolenic acid	Fatty acid	+	+	+	+
126	14.95	431.21958	$C_{21}H_{36}O_7P^-$	-1.9	402, 264, 152	PA(18:3)	Phosphatidic acid	+	+	+	+
127	15.53	847.4939	$C_{47}H_{75}O_{11}S^-$	-11.4	225, 165, 153, 95, 81	SQMG(38:8)	Sulfoglycolipid	+	+	-	+
128	15.57	483.2718	$C_{22}H_{44}O_9P^-$	-2.1	255, 152, 96, 78	PG(16:0/0:0)	Phosphatidyl glycerol	+	+	+	+
129	15.64	529.3008	$C_{27}H_{45}O_{10}^-$	-2.3	363, 279, 241	MGDG(18:2)	Glycolipid	+	+	-	+
130	15.83	295.2276	$C_{18}H_{31}O_3^-$	-0.8	295, 277, 183	Hydroxy octadecadienoic acid	Fatty acid	+	+	+	+
131	15.87	283.2634	$C_{18}H_{35}O_2^-$	-2.9	279, 205, 163, 138	Stearic acid	Fatty acid	-	-	-	+
132	15.97	815.4969	$C_{43}H_{75}O_{12}S^-$	-2	225, 165, 153, 95, 81	SQDG(34:3)	Sulfoglycolipid	-	-	-	+
133	16.06	433.2352	$C_{21}H_{38}O_7P^-$	-1.7	297, 275, 198, 152	PA(18:2)	Phosphatidic acid	+	+	+	+
134	16.10	853.4772	$C_{45}H_{73}O_{13}S^-$	-0.6	577, 225, 165, 153, 95, 81	SQDG(36:4)OH	Sulfoglycolipid	+	+	+	+
135	16.58	297.2433	$C_{18}H_{33}O_3^-$	-0.7	279, 239, 183, 155	Hydroxy oleic acid	Fatty acid	+	-	-	-
136	16.73	855.3847	$C_{45}H_{75}O_{13}S^-$	-1	577, 225, 165, 153, 95, 81	SQDG(36:5)OH	Sulfoglycolipid	+	+	-	-
137	17.02	249.1857	$C_{16}H_{25}O_2^-$	-1.1	205, 154, 112	Hexadecatrienoic acid	Fatty acid	+	+	+	+
138	17.06	311.2224	$C_{18}H_{31}O_4^-$	-1.2	223, 208, 151, 128, 87, 57	Dihydroxy octadecadienoic acid	Fatty acid	+	+	+	+
139	17.08	469.2586	$C_{28}H_{37}O_6^-$	-2	293, 275, 193, 175, 160, 148, 134, 114	Feruloyl oxylinolenic acid	Phenolic acid	+	+	-	-
140	17.09	149.0971	$C_{10}H_{13}O^-$	-0.4	133, 103, 79	Decatrienal	Aldehyde	+	+	-	-
141	17.40	811.4657	$C_{43}H_{71}O_{12}S^-$	-1.8	225, 165, 153, 95, 81	SQDG(34:5)	Sulfoglycolipid	+	-	-	-
142	17.41	809.4504	$C_{43}H_{69}O_{12}S^-$	-1.4	225, 165, 153, 95, 81	SQDG(34:6)	Sulfoglycolipid	+	+	-	-
143	17.53	831.5000	$C_{43}H_{76}O_{13}P^-$	-3.5	575, 277, 255, 241, 223, 152, 96, 78	PI(18:3/16:0)	Phosphatidyl inositol	+	-	+	-
144	18.05	833.5162	$C_{43}H_{78}O_{13}P^-$	-2.8	279, 255, 241, 223, 96, 78	PI(16:0/18:2)	Phosphatidyl inositol	-	+	-	+
145	18.37	853.4798	$C_{45}H_{74}O_{13}P^-$	-8.7	277, 241, 152	PI (18:3/18:3)	Phosphatidyl inositol	-	-	+	-
146	18.37	793.5125	$C_{41}H_{77}O_{12}S^-$	-2	225, 165, 153, 95, 81	SQDG(32:0)	Sulfoglycolipid	-	-	+	-
147	18.38	741.4694	$C_{40}H_{70}O_{10}P^-$	-2.1	277, 227, 152	PG(16:1/18:3)	Phosphatidyl glycerol	-	+	+	+
148	18.38	837.4816	$C_{45}H_{73}O_{12}S^-$	-1.3	225, 165, 153, 95, 81	SQDG(36:6)	Sulfoglycolipid	+	+	-	+

(continued on next page)

Table 1 (continued)

Peak num.	$t_r$ (min)	Molecular ion (M-H) (m/z)	Molecular ion formula	Error ppm	MS/MS fragments (m/z)	Identification	Compound class	Source			
								IR	IG	RR	RG
149	18.38	819.5240	C <sub>46</sub> H <sub>76</sub> O <sub>10</sub> P <sup>-</sup>	7.1	277, 152	PG(22:4/18:3)	Phosphatidyl glycerol	-	+	+	-
150	18.43	743.4847	C <sub>40</sub> H <sub>72</sub> O <sub>10</sub> P <sup>-</sup>	-2.9	279, 255, 227, 152	PG(18:2/16:1)	Phosphatidyl glycerol	-	-	-	+
151	18.44	277.2172	C <sub>18</sub> H <sub>29</sub> O <sub>2</sub>	-0.3	210, 159, 54	Linoleic acid	Fatty acid	+	+	+	+
152	18.5	271.2277	C <sub>18</sub> H <sub>31</sub> O <sub>3</sub>	-0.5	225, 170, 140	Hydroxy palmitic acid	Fatty acid	+	+	+	+
153	18.75	817.5127	C <sub>43</sub> H <sub>77</sub> O <sub>12</sub> S <sup>-</sup>	-1.7	225, 165, 153, 95, 81	SQDG(34:2)	Sulfoglycolipid	-	-	-	+
154	18.82	341.2688	C <sub>20</sub> H <sub>37</sub> O <sub>4</sub>	-2.7	281, 251, 224, 144, 70	Eicosanedioic acid	Fatty acid	+	+	+	+
155	19.01	787.4661	C <sub>41</sub> H <sub>71</sub> O <sub>12</sub> S <sup>-</sup>	-1.3	225, 165, 153, 95, 81	SQDG(32:3)	Sulfoglycolipid	+	+	-	-
156	19.04	813.4832	C <sub>43</sub> H <sub>75</sub> O <sub>12</sub> S <sup>-</sup>	0.5	225, 165, 153, 95, 81	SQDG(34:4)	Sulfoglycolipid	+	-	-	-
157	19.07	695.4641	C <sub>39</sub> H <sub>68</sub> O <sub>8</sub> P <sup>-</sup>	-2.3	281, 277, 182, 152	PA(18:3/18:1)	Phosphatidic acid	-	-	-	+
158	19.16	343.2848	C <sub>20</sub> H <sub>39</sub> O <sub>4</sub>	-1.6	311, 274, 259, 192, 120	Dihydroxy arachidic acid	Fatty acid	-	-	+	+
159	19.33	667.4333	C <sub>37</sub> H <sub>64</sub> O <sub>8</sub> P <sup>-</sup>	-1.7	413, 389, 277, 253, 171, 152, 78	PA(16:1/18:3)	Phosphatidic acid	+	+	-	-
160	19.33	693.4484	C <sub>39</sub> H <sub>66</sub> O <sub>8</sub> P <sup>-</sup>	-2.4	279, 277, 152, 78	PA(18:3/18:2)	Phosphatidic acid	+	-	-	-
161	19.33	841.5122	C <sub>45</sub> H <sub>77</sub> O <sub>12</sub> S <sup>-</sup>	-1.9	225, 165, 153, 95, 81	SQDG(36:4)	Sulfoglycolipid	+	+	-	-
162	19.35	839.4971	C <sub>45</sub> H <sub>75</sub> O <sub>12</sub> S <sup>-</sup>	-1.5	225, 165, 153, 95, 81	SQDG(36:5)	Sulfoglycolipid	+	-	-	+
163	19.70	313.2745	C <sub>19</sub> H <sub>37</sub> O <sub>3</sub>	-0.9	267, 247, 184	Hydroxy nonadecanoic acid	Fatty acid	-	-	+	+
164	19.72	791.4906	C <sub>44</sub> H <sub>72</sub> O <sub>10</sub> P <sup>-</sup>	4.8	277, 249, 223, 152	PG(18:3/20:4)	Phosphatidyl glycerol	-	+	+	-
165	19.72	691.4328	C <sub>39</sub> H <sub>64</sub> O <sub>8</sub> P <sup>-</sup>	-2.3	277, 152, 78	PA(18:3/18:3)	Phosphatidic acid	+	+	+	-
166	20.11	327.2909	C <sub>20</sub> H <sub>39</sub> O <sub>3</sub>	-0.7	183	Hydroxy eicosanoic acid	Fatty acid	-	-	+	+
167	20.39	669.4488	C <sub>37</sub> H <sub>66</sub> O <sub>8</sub> P <sup>-</sup>	-2.2	413, 409, 277, 255, 171, 152, 96, 78	PA(18:3/16:0)	Phosphatidic acid	+	+	+	-
168	20.39	695.4635	C <sub>39</sub> H <sub>68</sub> O <sub>8</sub> P <sup>-</sup>	-2.4	279, 152	PA(18:2/18:2)	Phosphatidic acid	+	+	+	-
169	20.40	671.4639	C <sub>37</sub> H <sub>68</sub> O <sub>8</sub> P <sup>-</sup>	-2.7	279, 255, 152, 78	PA(18:2/16:0)	Phosphatidic acid	-	+	+	+
170	20.40	843.5286	C <sub>45</sub> H <sub>79</sub> O <sub>12</sub> S <sup>-</sup>	-1.4	225, 165, 153, 95, 81	SQDG(36:3)	Sulfoglycolipid	-	+	+	-
171	21.99	825.4540	C <sub>43</sub> H <sub>70</sub> O <sub>13</sub> P <sup>-</sup>	-2.3	277, 259, 249, 241, 152, 78	PI(16:3/18:2)	Phosphatidyl inositol	+	+	-	-

Note. MGDG, monogalactosyldiacylglycerol; PA, phosphatidic acid; PG, phosphatidyl glycerol; PI, phosphatidyl inositol; SQDG, sulfoquinovosyl diacylglycerol, and SQMG, sulfoquinovosyl monoacylglycerol.

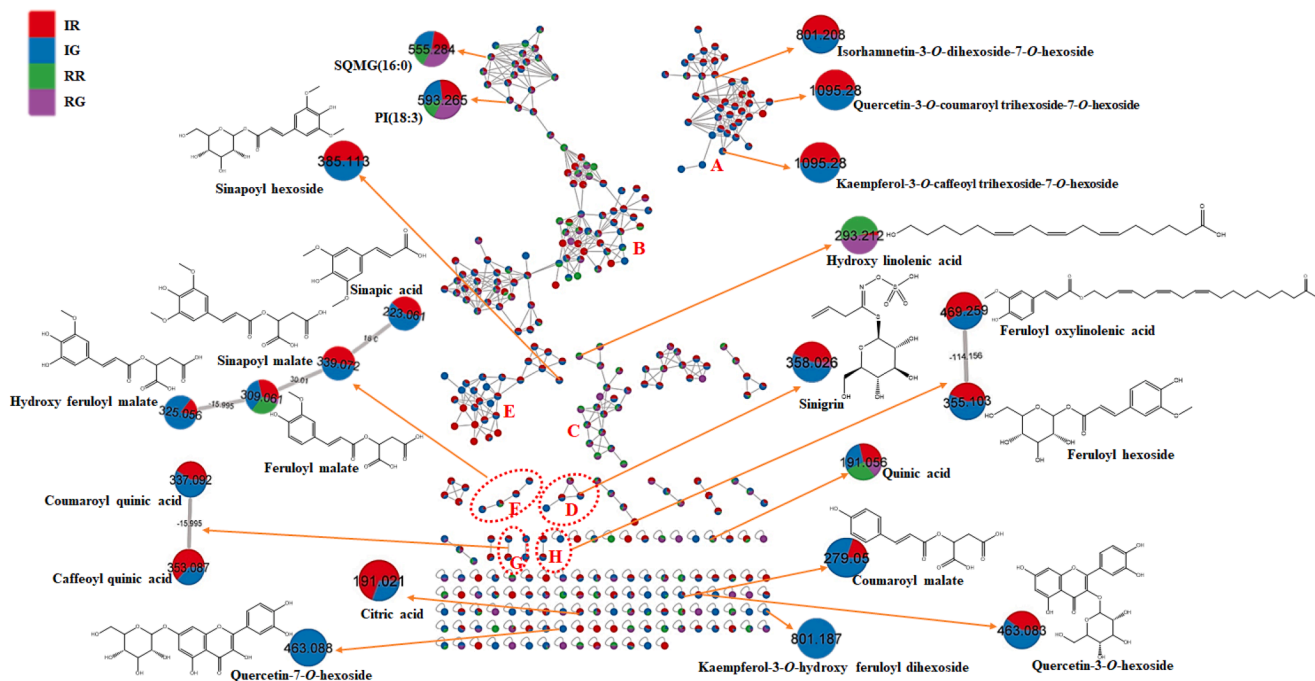


Fig. 1. MN established using MS/MS data in the negative ESI mode from the LC-QTOF-MS/MS analysis of mustard leaf extracts. The pie charts reflect the relative abundance of the detected molecular ions. Selected nodes and clusters have been zoomed in.

MS/MS spectra, they displayed a base peak at  $m/z$  133 due to the liberation of malate ion. Additionally, ten derivatives of sinapic acid were detected in the methanolic extracts of mustard leaves (Peaks 48, 66, 72, 84, 85, 86, 91, 92, 94, and 100, Table 1 and Fig. S7), and are mainly grouped in cluster E in the MN (Fig. 1). Finally, two hydroxybenzoic acids (3 and 19, Table 1) were also identified; protocatechuic acid and salicylic acid hexoside, with detected molecular ion peaks at  $m/z$  153.0192 and 299.0763, respectively, and showing fragments ions mainly due to dehydration and decarboxylation (Fig. S8 and S9).

### 3.2.3. Identification of flavonoids

Many flavonoids, including acylated and highly glycosylated compounds, have been previously reported in *Brassica* vegetables (cabbage, pak choi, broccoli, and mustard greens) (Lin & Harnly, 2010; Lin et al., 2011; Schmidt et al., 2010). Indeed, a great number of flavonoids were detected in our study. In total, forty-five flavonoids and their possible neutral losses in the MS/MS analysis are listed in Table 1. They comprised cluster B in the molecular network, as well as some self-looped nodes (Fig. 1). The identified flavonoids were mainly flavonols with quercetin, kaempferol, and isorhamnetin aglycones (Schmidt et al., 2010). The reported flavonol-O-glycosides were consistently glycosylated at either 3-OH and/or 7-OH positions (Ferrerres et al., 2009). While, the flavonol 4'-O-glycosides were reported to be comparatively rare in *Brassica* species (Farid et al., 2022).

**3.2.3.1. Identification of non-acylated flavonol glycosides.** Nineteen non-acylated flavonol glycosides were detected in mustard leaf extracts, including 7 kaempferol glycosides, 8 quercetin glycosides, 3 isorhamnetin glycosides, and 1 kaempferide glycoside. MS/MS-based MN could nicely differentiate between several flavonoids isomers and analogs as presented in Fig. 1. In Table 1, peaks 25, 35, 47, 67, 68, 81, and 82 were characterized as kaempferol glycosides, compounds 18, 21, 37, 58, 62, 70, 71, and 90 were assigned as quercetin glycosides, and peaks 40, 50, and 80 as isorhamnetin glycosides. Specifically, compounds 81 and 82 were identified as kaempferol-7-O-hexoside ( $m/z$  447.0922, Fig. S10) and kaempferol-3-O-hexoside ( $m/z$  447.0927, Fig. S11), respectively, through the relative abundances of the aglycone ions after the loss of the hexose moiety (-162 Da) (Farid et al., 2022).

**3.2.3.2. Identification of acylated flavonol glycosides.** Twenty-three acylated flavonol glycosides were detected, including 14 acylated kaempferol glycosides, 7 acylated quercetin glycosides, and 2 acylated isorhamnetin glycosides. They were found to lose their acyl group in MS/MS, characterized by the loss of 209  $m/z$  for hydroxyferuloyl, 162  $m/z$  for caffeoyl-, 206  $m/z$  for sinapoyl-, 176  $m/z$  for feruloyl-, and 146  $m/z$  for coumaroyl-derivatives, respectively (Table 1) (Schmidt et al., 2010). Peaks 20, 24, 28, 29, 38, 42, 45, 46, 51, 52, 53, 54, 69, and 75 were assigned as acylated kaempferol glycosides. For instance, compounds 20, 28, and 29 were found to be kaempferol glycosides acylated with caffeic acid. They displayed molecular ions at  $m/z$  933.2289 [ $C_{42}H_{45}O_{24}$ ], 1257.3330 [ $C_{54}H_{65}O_{34}$ ], and 1095.2840 [ $C_{48}H_{55}O_{29}$ ], respectively. In the MS/MS spectra, they showed fragment ions due to successive loss of hexose and dihexose units, in addition to the loss of caffeoyl radical (Sun et al., 2013). They were assigned as kaempferol-3-O-caffeoyl dihexoside-7-O-hexoside, kaempferol-3-O-caffeoyl trihexoside-7-O-dihexoside, and kaempferol-3-O-caffeoyl trihexoside-7-O-hexoside, respectively (Table 1). Similarly, kaempferol glycosides acylated with ferulic acid were detected in peaks 38, 45, and 51, while compounds 46, 54, and 75 were coumaroyl esters of kaempferol glycosides, peaks 52, 53, and 69 were annotated as kaempferol glycosides acylated with sinapic acid, and lastly compounds 24 and 42 were characterized as kaempferol glycosides acylated with hydroxyferulic acid (Table 1).

Similar to the detected kaempferol acylated glycosides, some quercetin derivatives were also annotated in peaks 26, 27, 30, 37, 30, 31, 33,

41, and 43, and two-acylated isorhamnetin glycosides were identified in peaks 74 and 83 (Table 1).

It is worth noting that the established MN (Fig. 1) was capable to discriminate ions from several flavonoid analogs with very close  $m/z$  values as observed for kaempferol-3-O-hydroxy feruloyl dihexoside (42) [ $m/z$  801.1870,  $C_{37}H_{37}O_{20}$ ], which appeared as a self-looped node separated from isorhamnetin-3-O-dihexoside-7-O-hexoside (40) [ $m/z$  801.2087,  $C_{34}H_{41}O_{22}$ ] in cluster A (Fig. 1). Furthermore, within the same cluster A (Fig. 1), compounds 29 and 30 were observed as two separate nodes having the same parent ion at  $m/z$  1095.2807 [ $M-H$ ]<sup>-</sup> as seen in Fig. 1. The inspection of their MS/MS spectra furthermore confirmed they had different fragmentation patterns and thus were identified as kaempferol-3-O-caffeoyl trihexoside-7-O-hexoside and quercetin-3-O-coumaroyl trihexoside-7-O-hexoside, respectively (Table 1).

### 3.2.4. Identification of lipids

Primary metabolites, e.g., lipids, fatty acids, and amino acids could affect relevant crop quality traits related to nutritional content and composition (Lisec et al., 2008). They are also fundamental to genetic improvement and metabolic engineering of plant primary production (Zhao et al., 2017). Fifty-four polar lipids were identified in the mustard leaf extracts that could be assigned to different chemical classes (i.e., phospholipids, glycolipids, and sulfolipids) based on their accurate molecular masses and characteristic fragmentation patterns. Interestingly, the MN (Fig. 1) unearthed their prevalence in the four mustard samples, and to the best of our knowledge; this is the first comprehensive insight into the lipid profile of *B. juncea* (L.) leaves.

Among phospholipids, metabolites ascribable to phosphatidylinositols (PI), phosphatidic acids (PA), and phosphatidylglycerols (PG), were putatively identified (Table 1). In particular, the analysis of peak 122 MS/MS spectrum [ $m/z$  599.3188,  $C_{27}H_{52}O_{12}P$ ] as an example for PI, revealed the presence of diagnostic product ions at nominal  $m/z$  315 and 241, corresponding to the dehydrated glycerophosphoinositol and inositol-phosphate ions, respectively (Table 1, Fig. S12). The ion at  $m/z$  283 corresponded to the 18:0 fatty acid carboxylate anion. Other characteristic ions were observed at nominal  $m/z$  259, 152, 96, and 78 corresponding to inositol phosphate, dehydrated glycerol-3-phosphate,  $H_2PO_4^-$ , and  $PO_3^-$  ions, respectively. Therefore, it was annotated as octadecanoyl-*sn*-glycero-3-phospho-(1'-myo-inositol) (PI(18:0)). Compound 167 [ $m/z$  669.4488,  $C_{37}H_{66}O_8P$ ], as a representative for PA, exhibited the diagnostic ions of phospholipids (nominal  $m/z$  171, 152, 96, and 78), and major ions at nominal  $m/z$  277 and 255 corresponding to the fatty acid carboxylate anions, respectively (Fig. S13). Accordingly, compound 167 was annotated as 1-(octadecatrienoyl)-2-hexadecanoyl-glycero-3-phosphate (PA(18:3/16:0)) (Okba et al., 2022). The MS/MS spectra of sulfolipids showed the typical product ion at  $m/z$  225, attributed to the sulfoquinovosyl anion. In addition to the specific ions at nominal  $m/z$  165, 153, and 95, the ion at nominal  $m/z$  81 resulted from the fragmentation of the sulfoquinovose group as seen in the MS/MS spectrum (Fig. S14) of peak 114 [ $m/z$  555.2837,  $C_{25}H_{47}O_{11}S$ ] (Table 1). As peak 114 exhibited the above fragment ions beside the hexadecanoic acid ion at  $m/z$  255, it was assigned as hexadecanoyl-3-(6'-sulfoquinovosyl)-*sn*-glycerol (SQMG (16:0)).

### 3.2.5. Identification of fatty acids and organic acids

Twenty-three fatty acids, mainly unsaturated and hydroxylated, such as dihydroxy octadecadienoic acid, linoleic acid, and hydroxy oleic acid, were identified in the mustard leaf extracts (Table 1). The diagnostic fragment ions generated by the loss of carbon dioxide and water molecules from the parent molecular ion were predominant in their spectra (Ibrahim et al., 2022).

Regarding the four identified organic acids, they appeared mainly as scattered nodes in the MN (Fig. 1) due to their characteristic fragmentation behavior. The observed fragmentation patterns were in agreement with the previous literature (Zhou et al., 2017). The MS/MS

spectra displayed abundant ions due to the loss of  $\text{CH}_2$ ,  $\text{CO}_2$ , and  $\text{H}_2\text{O}$  groups (Table 1). Quinic, citric, malic, and shikimic acids, were assigned based on their accurate masses, MS/MS fragmentation patterns, and reference data (Sun et al., 2013).

### 3.3. Antibacterial activity

All the mustard leaf extracts showed significant antibacterial activity against the tested Gram-positive bacteria (*S. aureus* and *E. faecalis*) ( $p < 0.001$ , using DMSO as negative control) (Fig. S15A-B). In contrast, none showed any inhibitory effect against the tested Gram-negative bacteria (Fig. S15C). For *S. aureus*, IR, IG, RR, and RG showed nearly close inhibition zones of  $27.0 \pm 1.7$  mm,  $26.0 \pm 2.0$  mm,  $25.6 \pm 1.5$  mm, and  $26 \pm 1.7$  mm, respectively (Fig. S15A). The same was also observed regarding *E. faecalis*, where the measured inhibition zones were  $23.7 \pm 5.0$  mm,  $23.67 \pm 3.2$  mm,  $23.7 \pm 4.0$  mm; and  $23.7 \pm 2.5$  mm for IR, IG, RR, and RG, respectively (Fig. S15B). In this last case, the observed antibacterial activity was not significantly different from the ciprofloxacin positive control ( $p > 0.7$ ). Indeed, mustard leaves contained a variety of antimicrobial compounds, including glucosinolates, flavonoids, and phenolic acids (Idrees, Tabassum, Sarah, & Hussain, 2019).

### 3.4. Antihemolytic activity

After confirming the antibacterial activity of the mustard leaf extracts against the tested Gram-positive bacteria, *S. aureus* was selected as a model to evaluate their antihemolytic activity. The results revealed that IR, IG, and RR were potent antihemolytic agents against *S. aureus* (Fig. 2). Whereas IR exhibited the highest antihemolytic effect (99 % inhibition), followed by RR (84 %), and IG (82 %). On the other hand, RG showed the least antihemolytic effect (~37 %), which was statistically non-significant ( $p = 0.86$ , Fig. 2). To the best of our knowledge, this is the first study reporting the antihemolytic potential of specific mustard leaves as a measurement of antivirulence.

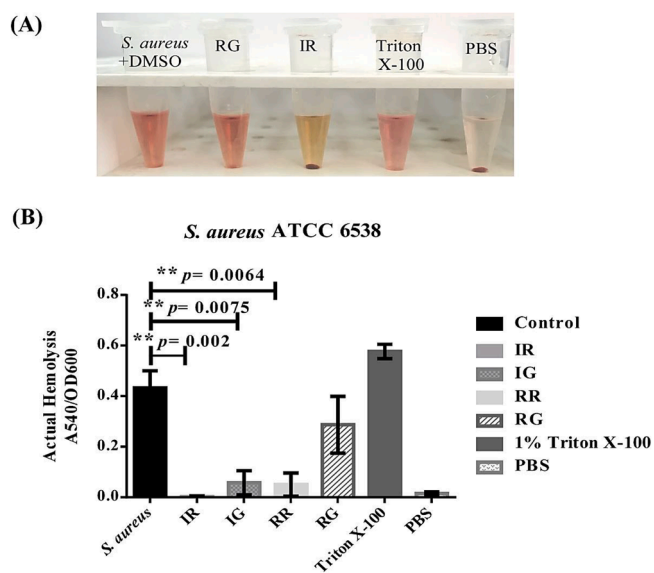


**Fig. 2.** Antihemolytic effect of sub-inhibitory concentrations of IR, IG, RR, and RG against *S. aureus* hemolysis. (A) A representative photograph of the anti-hemolytic effect determination for IR (significant effect), RG (no significant effect), *S. aureus* (with only DMSO), Triton X-100, and PBS. (B) The bar chart represents the actual hemolysis of the four extracts calculated by measuring the absorbance of released hemoglobin at 540 nm (A540), divided by the optical density of growth at 600 nm (OD600). The hemolytic activity of *S. aureus* culture (with only DMSO) was considered as a reference control. Asterisks (\*) indicate statistically significant differences (at  $p < 0.05$ ), in comparison to *S. aureus* as determined by ANOVA followed by post-hoc *t*-test.

### 3.5. Transcriptional analysis of *hla*

In concurrence with the great antihemolytic effect shown by the IR extract (99 % inhibition), a significant downregulation of *hla* transcriptional level of *S. aureus* was observed upon exposure to the extract (by 3.8 folds relative to the unexposed control (Fig. 3). In contrast, a minor and non-statistically significant reduction in *hla* transcriptional level (by ~ 1-fold) was observed for RG extract, in agreement with its weak antihemolytic effect (37 %). This phenotypic and genotypic differences illustrated the importance for the antihemolytic activity of certain chemical constituents in the IR extract, which may be absent or present at a different level in the RG extract.

### 3.6. Multivariate data analysis

The LC-MS analysis of the four mustard leaf extracts revealed that they had different chromatographic patterns, as shown in Fig. S1, Table 1, and highlighted by the MN (Fig. 1). Consequently, the LC-MS dataset was submitted to multivariate data analysis, to evaluate the chemical diversity and investigate the relative variability within the different mustard extracts in a more comprehensive and systematic manner (Younis et al., 2022). PCA and OPLS-DA were used to explore the data and build an untargeted classification of the four mustard leaf extracts, investigate the potential chemotaxonomic chemical markers for sample discrimination, and pinpoint the chemical constituents correlated to mustard bioactivities.

#### 3.6.1. Unsupervised analysis. PCA

PCA was performed to detect the metabolic differences or similarity among the four mustard leaf extracts, define classes, find outliers, and highlight the metabolites responsible for chemical variability (Fig. 4). Fig. 4A shows the PCA score plot with PC1 and PC2 accounting for 78.7 % of the explained variance. As can be observed, each extract type clustered together, confirming the repeatability of the extract preparation and the LC-MS analyses. The PCA score plot showed a clear separation of IR and IG extracts, along PC1 axis from each other, and along PC2 axis, from the RR and RG extracts, suggesting important differences in terms of metabolite profiles. In contrast, RR and RG were highly related and clustered together on the left side of the PC1 axis. The PCA loading plot (Fig. 4B) showed the metabolite contribution to the PC scores. The metabolites showing the largest absolute score values along each PC, which are colored in red and denoted by name if they were tentatively identified, were considered the most relevant to explain the

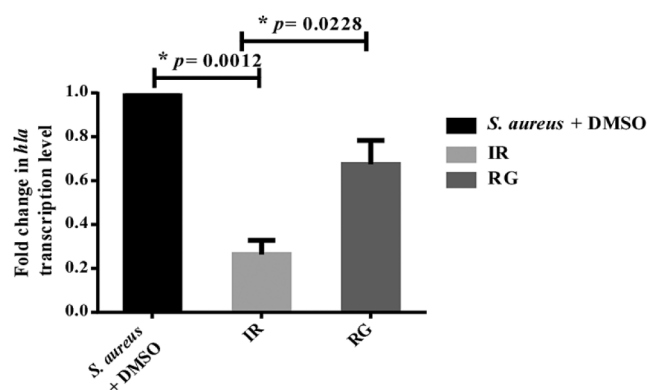


**Fig. 3.** Transcriptional analysis of *hla* gene of *S. aureus* upon exposure to sub-inhibitory concentrations of IR, and RG. The bar chart represents the fold change in the transcriptional level of *hla* gene upon exposure to IR or RG extracts. *S. aureus* culture (with only DMSO) was considered as control. Fold change was calculated using the  $\Delta\Delta\text{Ct}$  method. Asterisks (\*) indicate statistically significant differences (at  $p < 0.05$ ), in comparison to *S. aureus* as determined by ANOVA followed by post-hoc *t*-test.

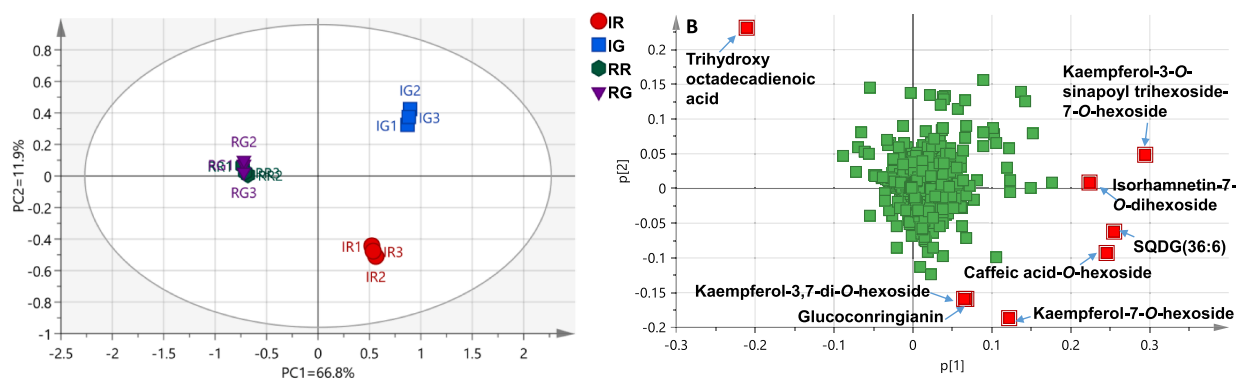


**Fig. 4.** (A) PCA score plot and (B) PCA loadings plot (the metabolites showing the largest absolute score values along each PC are named and colored in red if they were tentatively identified). Multivariate data analysis was performed with the complete LC-MS dataset. (For interpretation of the references to color in this figure legend, the reader is referred to the web version of this article.)

clusters observed in the PCA score plot. Accordingly, several metabolites, particularly phenolic compounds and glucosinolates, contributed to the separation of IR and IG from RR and RG samples (i.e., gluconringianin (12), SQDG(36:6) (148), kaempferol-3,7-di-O-hexoside (68), kaempferol-7-O-hexoside (81), isorhamnetin-7-O-dihexoside (50), kaempferol-3-O-sinapoyl trihexoside-7-O-hexoside (52), and caffeic acid-O-hexoside (77)). In addition, differences on the abundance of these metabolites would explain discrimination of IR and IG extracts. Regarding discrimination of RR and RG from IR and IG extracts, trihydroxy octadecadienoic acid (96) was found to be the most relevant metabolite.

### 3.6.2. Supervised analysis. OPLS-DA

OPLS-DA was performed to find the discriminating metabolites for each sample based on its variety and leaf color. Consequently, four OPLS-DA models were separately constructed with each extract, one at a time, against all other extracts. The first OPLS-DA score plot for IR extract modeled against the others (Fig. S16A) explained 99 % of the total variance ( $R^2 = 1$ ) with a prediction goodness parameter  $Q^2 = 0.99$ . The loadings S-plot (Fig. S16B) was used to compare the variable magnitude against its reliability, where axes plotted from the predictive component were the covariance P[1] against the correlation P(cor)[1]. Loadings S-plot is particularly useful to visualize the most relevant metabolites for the discrimination (Wiklund, 2008; Younis et al., 2022). Eight discriminating metabolites were predominant in IR extract compared to the others, including gluconringianin (12), caffeic acid-O-hexoside (77), kaempferol-7-O-hexoside (81), kaempferol-3,7-di-O-hexoside (68), isorhamnetin-3-O-dihexoside-7-O-hexoside (40), isorhamnetin-7-O-dihexoside (50), kaempferol-3-O-sinapoyl trihexoside-7-O-hexoside (52), and SQDG(36:6) (148). The second OPLS-DA score plot for IG extract modeled against the others (Fig. S16C) showed also good quality parameters ( $R^2 = 1$  and  $Q^2 = 0.99$ ). The loadings S-plot (Fig. S16D) revealed that IG extract was particularly discriminated from the others by isorhamnetin-7-O-dihexoside (50), caffeic acid-O-hexoside (77), kaempferol-3-O-sinapoyl trihexoside-7-O-hexoside (52), kaempferol-3-O-coumaroyl dihexoside-7-O-dihexoside (46), quercetin-3-O-dihexoside (37), hydroxyferulic acid (57), sinigrin (1), and SQDG(36:6) (148). The remaining two OPLS-DA models (Fig. S17A-D) were similarly constructed for the RR and RG extracts ( $R^2 = 1$  and  $Q^2 = 0.99$ ). In the two models, trihydroxy octadecadienoic acid (96) was a relevant metabolite for discrimination of both samples according to the loadings S-plots (Figs. S17B and 17D), in agreement with the previous observations made by PCA (Fig. 4B). In addition, hydroxy palmitic acid (152) and hydroxy oxo-octadecatrienoic acid (107) were the discriminating metabolites of the RR and RG extracts, respectively (Figs. S17B and 17D, respectively). The four OPLS-DA models were validated for their ability to correlate the metabolite profiles of the different extracts using

permutation testing (100 iterations), with negative  $Q^2$  intercept value (Figs. S18A-21A) indicating model validity and the absence of data overfitting. The receiver operating characteristic (ROC) curve obtained for each model passed through the upper left corner (100 % selectivity, 100 % sensitivity) and the area under the ROC curve (AUC) was considered as a validation criterion for model classification and was found to be 1.0, indicating that the model was highly effective for group separation by the obtained variables (Figs. S18B-21B) (Otify et al., 2023). Moreover, the four models showed low cross-validation residuals (CV-ANOVA), root mean square error of estimation (RMSEE), and root mean square error of cross-validation (RMSEcv) values (Figs. S18C-21C), indicating high accuracy and good prediction power of each model (Younis et al., 2022). Overall, the OPLS-DA results confirmed the PCA results, indicating that the differences in the abundance and type of glucosinolates and phenolic compounds accounted mainly for IR and IG leaves segregation, whereas fatty acids, particularly trihydroxy octadecadienoic acid (96), predominated in RR and RG leaves.

### 3.6.3. Metabolites-bioactivity correlation

**3.6.3.1. Correlation with antibacterial activity against the different bacterial strains.** Pearson's correlation coefficients were employed to find out the relationship between the abundance of the 171 identified metabolites in the different mustard leaf extracts (Table 1) and the antibacterial activity, where Pearson's correlation coefficient ( $r$ ) was  $\geq 0.7$  at  $p < 0.05$  and false discovery rate (FDR)  $< 0.08$ . The top 25 metabolites that positively correlated mustard extracts with the antibacterial activity included flavonoids, phenolic acids, glucosinolates, and isothiocyanates. While compounds that were negatively correlated with the antibacterial activity were mostly fatty acids and lipids (Fig. 5A, Table S2). Most of the positively correlated biomarker metabolites were reported to exert antibacterial activity against various strains of Gram-positive bacteria such as sinigrin and allyl isothiocyanate (Mazumder, Dwivedi, & Du Plessis, 2016). Moreover, several reports were found regarding the antimicrobial activity of positively correlated flavonoids and phenolic acids such as isorhamnetin, cinnamic, and *p*-coumaric acids (Gong et al., 2020; Sova, 2012). Our results were in agreement with previous studies on the antibacterial activity of mustard leaves (Verma et al., 2022).

**3.6.3.2. Correlation with antihemolytic activity against *S. aureus*.** Correlation analysis between the abundance of the 171 identified metabolites in the four analyzed mustard leaf extracts and antihemolytic activity, revealed certain relationships (Pearson's correlation coefficient ( $r$ ) was  $\geq 0.7$  at  $p < 0.05$  and  $FDR \leq 0.08$ , Table S3, Fig. 5B). Additionally, the metabolites discriminating between the active and inactive samples were additionally confirmed by calculating the VIP scores obtained from

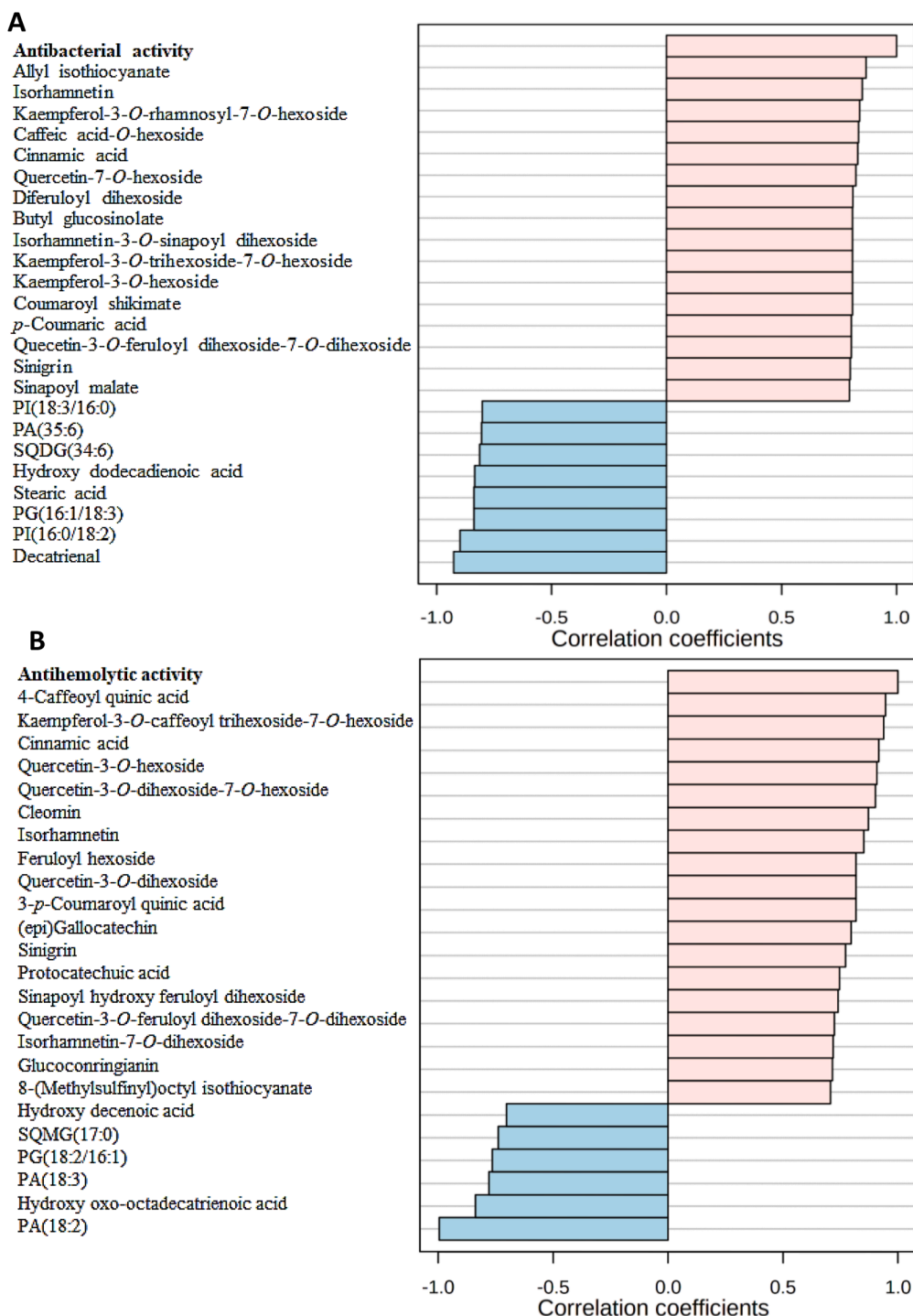


**Fig. 5.** Top 25 metabolites of the 171 identified metabolites correlated with (A) the antibacterial activity and (B) the antihemolytic activity of the mustard leaf extracts (IR, IG, RR, and RG). The details of the biomarker metabolites are listed in Tables S2-S3.

the OPLS-DA modelling ( $R^2 = 0.99$  and  $Q^2 = 0.94$ ) of the active extracts (IR, IG, and RR) against the inactive one (RG extract) (Fig. S22). As can be observed, the discriminating metabolites were considered to be relevant to explain the variance when also having VIP scores  $> 1$  at  $p < 0.05$  (Table S3, Fig. S22B). The biomarker metabolites positively correlated to the antihemolytic activity were flavonoids (kaempferol-3-*O*-caffeoyl trihexoside-7-*O*-hexoside (29), kaempferol-3-*O*-sinapoyl trihexoside-7-*O*-hexoside (52), quercetin-3-*O*-hexoside (71), quercetin-3-*O*-dihexoside-7-*O*-hexoside (21), quercetin-3-*O*-feruloyl dihexoside-7-*O*-dihexoside (26), isorhamnetin (101), and isorhamnetin-7-*O*-

dihexoside (50)), and phenolic acids (4-caffeoyl quinic acid (36), cinnamic acid (14), feruloyl hexoside (61), protocatechuic acid (3), sinapoyl hydroxy feruloyl dihexoside (72), and 3-*p*-coumaroyl quinic acid (60)). Glucosinolates (sinigrin (1) and glucoconringianin (12)), and isothiocyanates (cleomin (16) and 8-(methylsulfinyl)octyl isothiocyanate (13)) were also positively correlated with the antihemolytic activity along with the flavanol (*epi*)gallocatechin (17) (Fig. 5B). The abundance of the interesting biomarker compounds leading to the discrimination of the active and inactive extracts can be observed in Fig. S22B. All of them showed higher abundance in the three active leaf

extracts (IR, IG, and RR). Lastly, it was obvious that the inactive RG sample had lower levels of the bioactive compounds besides its enrichment in fatty acids and lipids (PA(18:2) (**133**), PA(18:3) (**126**), hydroxy oxo-octadecatrienoic acid (**107**), SQMG(17:0) (**119**), PG(18:2/16:1) (**150**), and hydroxy decenoic acid (**106**)), which have high negative correlations with the antihemolytic activity of RG extract (Table S3, Fig. 5B and S22B). Accordingly, these findings could explain the significant downregulation that was observed in staphylococcal *hla* transcription upon exposure to IR extract rather than RG extract.

Interestingly, previous reports revealed that several phenolic acids and flavonoids exert potent antibacterial and antivirulence activities (Okba et al., 2022; Silva, Zimmer, Macedo, & Trentin, 2016). They could interfere with the quorum sensing system (responsible for the expression of several virulence genes), and disrupt bacterial signaling. Different glycosides of kaempferol and quercetin, as well as isorhamnetin have exhibited potent antibiofilm activities against several bacterial strains, besides supporting the reduction of hemolysis (Silva et al., 2016). In addition, several reports confirmed the antibacterial and antivirulence activities of cinnamic acid and epigallocatechin (Okba et al., 2022; Silva et al., 2016). Glucosinolates and isothiocyanates, such as sinigrin and allyl isothiocyanate, have been related to antiquorum sensing, anti-hemolytic, and antibiofilm activities (Mazumder et al., 2016). Additionally, previous studies showed the capability of protocatechuic acid to inhibit the growth of various bacteria, besides the downregulation of important virulence gene regulators (Alvarado-Martinez et al., 2020). It is worth noting that, many mustard metabolites presented a well-documented antivirulence potency and contributed to the anti-hemolytic activity. This comes in concurrent agreement with our results that illustrated the potent antibacterial activity and antihemolytic effect of mustard extracts, especially against *S. aureus*.

#### 4. Conclusion

As far as the authors are aware, this is the first full comparative metabolic profiling of red and green mustard leaves of two *B. juncea* (L.) varieties, var. *integrifolia* and var. *rugosa* by untargeted LC-QTOF-MS/MS metabolomics assisted with MN and multivariate data analysis. LC-QTOF-MS/MS allowed to obtain comprehensive chemical profiles of the four mustard extracts, where 171 were tentatively identified after a careful interpretation of the data, including MN with GNPS that provided deeper insights into mustard leaves metabolome. Then, multivariate data analysis revealed the compositional similarities and differences in primary and secondary metabolites among the four mustard leaf extracts. All mustard leaves demonstrated significant antibacterial activity against Gram-positive bacteria *S. aureus* and *E. faecalis*, with IR, IG, and RR exhibiting great antihemolytic effect, hence antivirulence activity, against *S. aureus*. Different data analysis tools positively correlated various phenolic compounds, glucosinolates, and isothiocyanates to the antibacterial and antivirulence activities. Accordingly, more focus should be directed towards these leaves to be further examined as possible natural sources of antibacterial agents, especially IR that demonstrated a significant antivirulence activity diminishing the staphylococcal hemolytic activity and reducing *hla* transcription. However, it should be noted that these findings are preliminary, and further research with the raw leaf extracts or after purification of specific compounds, followed by more detailed and conclusive *in vivo* and clinical studies, are highly recommended to exploit mustard leaf potential in agri-food and pharmaceutical industries.

#### CRediT authorship contribution statement

**Rana M. Ibrahim:** Conceptualization, Methodology, Investigation, Formal analysis, Validation, Data curation, Visualization, Writing – original draft. **Basma Eltanany:** Methodology, Formal analysis, Validation, Data curation, Writing – review & editing. **Laura Pont:**

Methodology, Writing – review & editing. **Fernando Benavente:** Supervision, Writing – review & editing. **Shahira AbdelSalam ElBanna:** Conceptualization, Methodology, Investigation, Formal analysis, Validation, Data curation, Visualization, Writing – original draft. **Asmaa M. Otfy:** Conceptualization, Methodology, Visualization, Writing – review & editing.

#### Declaration of Competing Interest

The authors declare that they have no known competing financial interests or personal relationships that could have appeared to influence the work reported in this paper.

#### Data availability

Data will be made available on reasonable request

#### Acknowledgment

Basma M. Eltanany would like to thank the Egyptian Ministry of Higher Education for funding her postdoc research stay with the Bio-analysis group at the University of Barcelona, Barcelona, Spain.

Shahira A. ElBanna would like to thank the following members of the Microbiology and Immunology department (Faculty of Pharmacy, Cairo University) for sharing different bacterial strains through the department library, starting with professor Dr. Ahmed S. Attia, associate professors Dr. Reham Samir, and Dr. Maha M. Ismail, in addition to Dr. Yomna A. Hashem, lecturer of the Microbiology and Immunology department (Faculty of Pharmacy, The British University in Egypt) and Dr. Nahla Hussein, researcher of the Molecular Biology department (National Research Centre).

#### Funding source

This research had no specific funding sources.

#### Appendix A. Supplementary material

Supplementary data to this article can be found online at <https://doi.org/10.1016/j.foodres.2023.112742>.

#### References

- Alvarado-Martinez, Z., Bravo, P., Kennedy, N.-F., Krishna, M., Hussain, S., Young, A. C., & Biswas, D. (2020). Antimicrobial and antivirulence impacts of phenolics on *Salmonella enterica* serovar Typhimurium. *Antibiotics*, 9(10), 668. <https://doi.org/10.3390/antibiotics9100668>
- Andini, S., Araya-Cloutier, C., Lay, B., Vreeke, G., Hageman, J., & Vincken, J.-P. (2021). QSAR-based physicochemical properties of isothiocyanate antimicrobials against gram-negative and gram-positive bacteria. *LWT*, 144, Article 111222. <https://doi.org/10.1016/j.lwt.2021.111222>
- Cuong, D. M., Kim, J. K., Bong, S. J., Baek, S. A., Jeon, J., Park, J. S., & Park, S. U. (2018). Comparative analysis of glucosinolates and metabolite profiling of green and red mustard (*Brassica juncea*) hairy roots. *3 Biotech*, 8(9), 1–10. <https://doi.org/10.1007/s13205-018-1393-x>
- Esteve, M. (2020). Mechanisms underlying biological effects of cruciferous glucosinolate-derived isothiocyanates/indoles: A focus on metabolic syndrome. *Frontiers in Nutrition*, 7, 111. <https://doi.org/10.3389/fnut.2020.00111>
- Farid, M. M., Ibrahim, F. M., Ragheb, A. Y., Mohammed, R. S., Hegazi, N. M., Shabrawy, M. O. E., ... Marzouk, M. M. (2022). Comprehensive phytochemical characterization of *Raphanus raphanistrum* L.: In vitro antioxidant and antihyperglycemic evaluation. *Scientific African*, 16. <https://doi.org/10.1016/j.sciaf.2022.e01154>
- Ferreres, F., Fernandes, F., Oliveira, J. M., Valentão, P., Pereira, J. A., & Andrade, P. B. (2009). Metabolic profiling and biological capacity of *Pieris brassicae* fed with kale (*Brassica oleracea* L. var. *acephala*). *Food Chemical Toxicology*, 47(6), 1209–1220. <https://doi.org/10.1016/j.fct.2009.02.014>
- Gonellimali, F. D., Lin, J., Miao, W., Xuan, J., Charles, F., Chen, M., & Hatab, S. R. (2018). Antimicrobial Properties and Mechanism of Action of Some Plant Extracts Against Food Pathogens and Spoilage Microorganisms. *Frontiers in Microbiology*, 9, 1639. <https://doi.org/10.3389/fmicb.2018.01639>
- Gong, G., Guan, Y.-Y., Zhang, Z.-L., Rahman, K., Wang, S.-J., Zhou, S., ... Zhang, H. (2020). Isorhamnetin: A review of pharmacological effects. *Biomedicine Pharmacotherapy*, 128, Article 110301. <https://doi.org/10.1016/j.biopha.2020.110301>

- Grumann, D., Nubel, U., & Broker, B. M. (2014). Staphylococcus aureus toxins—their functions and genetics. *Infection, Genetics and Evolution*, 21, 583–592. <https://doi.org/10.1016/j.meegid.2013.03.013>
- Hegazi, N. M., Khattab, A. R., Frolow, A., Wessjohann, L. A., & Farag, M. A. (2022). Authentication of saffron spice accessions from its common substitutes via a multiplex approach of UV/VIS fingerprints and UPLC/MS using molecular networking and chemometrics. *Food Chemistry*, 367, Article 130739. <https://doi.org/10.1016/j.foodchem.2021.130739>
- Humphries, R. M., Ambler, J., Mitchell, S. L., Castanheira, M., Dingle, T., Hindler, J. A., ... Sei, K. (2018). CLSI methods development and standardization working group best practices for evaluation of antimicrobial susceptibility tests. *Journal of Clinical Microbiology*, 56(4), e01917–e01934. <https://doi.org/10.1128/JCM.01934-17>
- Ibrahim, R. M., Elmasry, G. F., Refaey, R. H., & El-Shiekh, R. A. (2022). Lepidium meyenii (Maca) Roots: UPLC-HRMS, Molecular Docking, and Molecular Dynamics. *ACS Omega*. <https://doi.org/10.1021/acsomega.2c01342>
- Ildrees, N., Tabassum, B., Sarah, R., & Hussain, M. K. (2019). Natural compound from genus brassica and their therapeutic activities. In *Natural bio-active compounds* (pp. 477–491). Springer.
- Jaiswal, A. K., Rajauria, G., Abu-Ghannam, N., & Gupta, S. (2012). Effect of different solvents on polyphenolic content, antioxidant capacity and antibacterial activity of Irish York cabbage. *Journal of Food Biochemistry*, 36(3), 344–358. <https://doi.org/10.1111/j.1745-4514.2011.00545.x>
- Jaiswal, R., Sovdat, T., Vivan, F., & Kuhnert, N. (2010). Profiling and characterization by LC-MS n of the chlorogenic acids and hydroxycinnamoylshikimate esters in mate (Ilex paraguariensis). *Journal of Agricultural Food Chemistry*, 58(9), 5471–5484. <https://doi.org/10.1021/jf904537z>
- Jo, S. H., Cho, C. Y., Ha, K. S., Lee, J. Y., Choi, H. Y., Kwon, Y. I., & Apostolidis, E. (2018). In vitro and in vivo anti-hyperglycemic effects of green and red mustard leaves (Brassica juncea var. integrifolia). *Journal of Food Biochemistry*, 42(5). <https://doi.org/10.1111/jfbc.12583>. e12583.
- Jouaneh, T. M. M., Motta, N., Wu, C., Coffey, C., Via, C. W., Kirk, R. D., & Bertin, M. J. (2022). Analysis of botanicals and botanical supplements by LC-MS/MS-based molecular networking: Approaches for annotating plant metabolites and authentication. *Fitoterapia*, 159, Article 105200. <https://doi.org/10.1016/j.fitote.2022.105200>
- Kim, H., Kim, J.-Y., Kim, H.-J., Kim, D.-K., Jo, H.-J., & Han, B.-S. (2011). ... Anticancer activity and quantitative analysis of glucosinolates from green and red leaf mustard. *The Korean Journal of Food Nutrition*, 24(3), 362–366. <https://doi.org/10.9799/ksfan.2011.24.3.362>
- Kumar, N., & Pruthi, V. (2014). Potential applications of ferulic acid from natural sources. *Biotechnology Reports*, 4, 86–93. <https://doi.org/10.1016/j.btre.2014.09.002>
- Lin, L.-Z., & Harnly, J. M. (2010). Phenolic component profiles of mustard greens, yu choy, and 15 other Brassica vegetables. *Journal of Agricultural Food Chemistry*, 58(11), 6850–6857. <https://doi.org/10.1021/jf1004786>
- Lin, L.-Z., Sun, J., Chen, P., & Harnly, J. (2011). UHPLC-PDA-ESI/HRMS/MS<sup>n</sup> analysis of anthocyanins, flavonol glycosides, and hydroxycinnamic acid derivatives in red mustard greens (Brassica juncea Coss variety). *Journal of Agricultural Food Chemistry*, 59(22), 12059–12072. <https://doi.org/10.1021/jf202556p>
- Liseac, J., Meyer, R. C., Steinfath, M., Redestig, H., Becher, M., Witucka-Wall, H., ... Altmann, T. (2008). Identification of metabolic and biomass QTL in Arabidopsis thaliana in a parallel analysis of RIL and IL populations. *The Plant Journal*, 53(6), 960–972. <https://doi.org/10.1111/j.1365-313X.2007.03383.x>
- Livak, K. J., & Schmittgen, T. D. (2001). Analysis of relative gene expression data using real-time quantitative PCR and the 2(-Delta Delta C(T)) Method. *Methods*, 25(4), 402–408. <https://doi.org/10.1006/meth.2001.1262>
- Mazumder, A., Dwivedi, A., & Du Plessis, J. (2016). Sinigrin and its therapeutic benefits. *Molecules*, 21(4), 416. <https://doi.org/10.3390/molecules21040416>
- Merah, O. (2015). Genetic variability in glucosinolates in seed of Brassica juncea: interest in mustard condiment. *Journal of Chemistry*, 2015. <https://doi.org/10.1155/2015/606142>
- Okba, M. M., Baki, P. M. A., Abu-Elghait, M., Shehabeldine, A. M., El-Sherei, M. M., Khaleel, A. E., & Salem, M. A. (2022). UPLC-ESI-MS/MS profiling of the underground parts of common Iris species in relation to their anti-virulence activities against Staphylococcus aureus. *Journal of Ethnopharmacology*, 282, Article 114658. <https://doi.org/10.1016/j.jep.2021.114658>
- Otify, A. M., Ibrahim, R. M., Abib, B., Laub, A., Wessjohann, L. A., Jiang, Y., & Farag, M. A. (2023). Unveiling metabolome heterogeneity and new chemicals in 7 tomato varieties via multiplex approach of UHPLC-MS/MS, GC-MS, and UV-Vis in relation to antioxidant effects as analyzed using molecular networking and chemometrics. *Food Chemistry*, 135866. <https://doi.org/10.1016/j.foodchem.2023.135866>
- Saavedra, M. J., Borges, A., Dias, C., Aires, A., Bennett, R. N., Rosa, E. S., & Simões, M. (2010). Antimicrobial activity of phenolics and glucosinolate hydrolysis products and their synergy with streptomycin against pathogenic bacteria. *Medicinal Chemistry*, 6(3), 174–183. <https://doi.org/10.2174/1573406411006030174>
- Schmidt, S., Zietz, M., Schreiner, M., Rohn, S., Kroh, L. W., & Krumbain, A. (2010). Identification of complex, naturally occurring flavonoid glycosides in kale (Brassica oleracea var. sabellica) by high-performance liquid chromatography diode-array detection/electrospray ionization multi-stage mass spectrometry. *Rapid Communications in Mass Spectrometry*, 24(14), 2009–2022. <https://doi.org/10.1002/rcm.4605>
- Silva, L. N., Zimmer, K. R., Macedo, A. J., & Trentin, D. S. (2016). Plant Natural Products Targeting Bacterial Virulence Factors. *Chemical Reviews*, 116(16), 9162–9236. <https://doi.org/10.1021/acs.chemrev.6b00184>
- Song, L., Iori, R., & Thornalley, P. J. (2006). Purification of major glucosinolates from Brassicaceae seeds and preparation of isothiocyanate and amine metabolites. *Journal of the Science of Food and Agriculture*, 86(8), 1271–1280. <https://doi.org/10.1002/jsfa.2488>
- Sova, M. (2012). Antioxidant and antimicrobial activities of cinnamic acid derivatives. *Mini Reviews in Medicinal Chemistry*, 12(8), 749–767. <https://doi.org/10.2174/138955712801264792>
- Sun, J., Xiao, Z., Lin, L.-Z., Lester, G. E., Wang, Q., Harnly, J. M., & Chen, P. (2013). Profiling polyphenols in five Brassica species microgreens by UHPLC-PDA-ESI/HRMS n. *Journal of Agricultural Food Chemistry*, 61(46), 10960–10970. <https://doi.org/10.1021/jf401802n>
- Tian, Y., & Deng, F. (2020). Phytochemistry and biological activity of mustard (Brassica juncea): A review. *CyTA-Journal of Food*, 18(1), 704–718. <https://doi.org/10.1080/19476337.2020.1833988>
- Tian, Y., Deng, F., Zhao, L., Du, H., Li, T., Lai, D., ... Qing, Z. (2021). Characterization of extractable components of fresh and fermented Huarong large-leaf mustard and their inhibitory effects on human colon cancer cells. *Food Bioscience*, 43, Article 101280. <https://doi.org/10.1016/j.fbio.2021.101280>
- Verma, S., Tiwari, B. K., Jaiswal, N., & Pandey, F. K. (2022). Evaluation of antimicrobial activity of Brassica juncea leaves against different strains of bacteria. *Bio Science Research Bulletin*, 38(1), 26–34. <https://doi.org/10.5958/2320-3161.2022.00003.7>
- Wiklund, S. (2008). Multivariate data analysis for Omics. *Umea: Umetrics*, Sweden, pp 108–109. Available online: <https://metabolomics.se/Courses/MVA/MVA%20in%20Omics/Handouts/Exercises/Thu-Fri.pdf> (accessed on 3/2023).
- Younis, I. Y., Ibrahim, R. M., El-Halawany, A. M., Hegazy, M.-E.-F., Efferth, T., & Mohsen, E. (2022). Chemometric discrimination of Hylcoereus undulatus from different geographical origins via their metabolic profiling and antidiabetic activity. *Food Chemistry*, 134650. <https://doi.org/10.1016/j.foodchem.2022.134650>
- Zhang, S., Li, C., Gu, W., Qiu, R., Chao, J., Pei, L., Ma, L., Guo, Y., & Tian, R. (2021). Metabolomics analysis of dandelions from different geographical regions in China. *Phytochemical Analysis*. <https://doi.org/10.1002/pca.3033>
- Zhao, S.-Y., Liu, Z.-L., Shu, Y.-S., Wang, M.-L., He, D., Song, Z.-Q., ... Lu, A.-P. (2017). Chemotaxonomic classification applied to the identification of two closely-related Citrus TCMS using UPLC-Q-TOF-MS-based metabolomics. *Molecules*, 22(10), 1721. <https://doi.org/10.3390/molecules22101721>
- Zhou, Y., Li, P., Brantner, A., Wang, H., Shu, X., Yang, J., ... Bian, B. (2017). Chemical profiling analysis of Maca using UHPLC-ESI-Orbitrap MS coupled with UHPLC-ESI-Qq MS and the neuroprotective study on its active ingredients. *Scientific reports*, 7(1), 1–14. <https://doi.org/10.1038/srep44660>